ELECTRICAL CONDUCTION IN AMORPHOUS TRINITRO-NINE-FLUORENONE AND SELENIUM

BY
MEKONNEN ABEBE

A thesis submitted in partial fulfillment for the degree
Master of Science in Physics
in Addis Ababa University.

June 1992

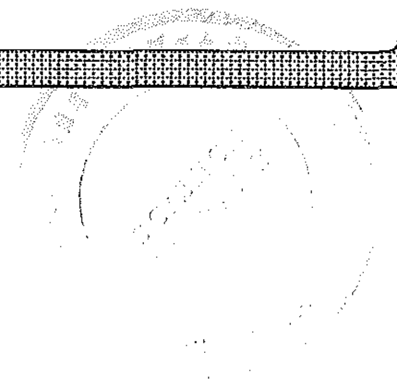

Mek
phy
1992

ACKNOWLEDGEMENTS

Most of all I am very grateful to my Advisor Dr. I.M. Kashiriski with whom I have had the pleasure of working on diverse aspects of research on electrical conductions in a-TNF and a-se. I wish to express my appreciation to Dr. I.M. Kashiriski whose indespensable help and patient encouragement made this work possible.

Finally, I am indebted to many of the staff and colleagues at the Department of Physics in AAU. I am especially grateful to Ato Girma Dagne for his remarkable efforts to cope with technical part of the thesis.

ABSTRACT

The theories of electronic structures in amorphous semiconductors are reviewed. The effectiveness of the study of electrical conductions particularly the SCLC, TSC and transient photoconductivity, in providing a wealth of information on electronic properties of disordered solids also discussed. Analytic equations describing the above three conduction properties are also developed. Experimental study of the SCLC, TSC and transient photoconductivity is made for a_TNF and a-Se.

Distinctly from the models that are based on the assumptions of discrete or uniform distributions of traps in energy, our experimental works on a-TNF and a-Se indicate the existence of energetically dispersed charge carriers trapping states. The observed space charge limited mode of conduction and its temperature sensitivity is found to be best describable interms of a smoothly varying distributions. The Gaussian distribution seems more realistic for the interpretation of experimental results in a-TNF and a-Se.

Both hopping and multiple trapping models are used in interpreting the transient photo-conductivity experimental results for a-TNF and a-Se respectively. Drift mobilities of charge carriers are seen to exhibit an activated nature and also found to be field dependent in a manner similar to the poole-Frenkel mechanism. For an explanation of the dispersive hole transport in a-Se interms of the multiple trapping model, the theoretical predictions developed on the basis of a Gaussian distribution is found to agree with experimental results more satisfactorily.

The study of thermally stimulated current characteristics in a-TNF near the glass transition temperature, Tg, renders an activation energy which is significantly different from results of low temperature TSC analysis. Rather, it is nearly identical to the zero field extrapolated activation energy computed from transient photo conductivity experiments. There by indicates this energy parameters to contain the disorder induced term.

CONTENTS

PAGE

INTRODUCTION 1

CHAPTER I 4

1. A review of electronic structure in amorphous semiconductors.............................. 4

1.1 Bonding and structure in A-semiconductors 4

1.2 Native defects and associated states 7

CHAPTER II 11

2. Steady state space charge limited current 11

2.1 Analytical equations for SCLC 11

2.1a Monoenergetic traps 14

2.1b Exponential distribution 15

2.1c Gaussian distribution 18

2.2 Applicability of SCLC analytical equations 21

CHAPTER III

3. Dispersive transport in amorphous semiconductors 26

3.1 Microscopic mechanisms underlying dispersive transport 26

3.2 Hopping conduction 30

3.3 Multiple trapping model.................. 38

CHAPTER IV 52

4. Thermlly stimulated current in amorphous semiconductors 52

4.1 Classical TSC equations 52

4.2 Field dependent TSC 56

4.3 TSC around the glass transition temperature (Tg) 59

CHAPTER V 64

5 Electrical conduction experiments 64

5.1 SCLC experiments 66

PAGE

5.2 Transient photoconductivity experiments ... 78

5.3 TSC experiments 92

5.4 Summary and conclusions 95

APPENDIX A 101

APPENDIX B 103

APPENDIX C 110

APPENDIX D 112

BIBLIOGRAPHY

ADDIS ABABA UNIVERSITY LIBRARIES

INTRODUCTION

Amorphous semiconductors comprises covalentely bonded disordered solids. They exhibit electrical and magnetic properties very different from their crystalline counter-parts. This enables them to be the best candidates for applications in the fields of electrophtography, solar energy conversion, space and air flight, computer memory elements, tele-comunications (glass fibers), in protecting from infrared detectability (military purposes), and as gas sensors[1-4]. The posobility of use as biosensors[3], for making internally powered artificial heart and artificial nerves perhaps even modification to the brain are amongst the likely future applications of a-semiconductors: especially polymers.

Therefore, evidently enormous research works have been gravitated since the early discovery of electrophtography at the begining of 1940s[2]. One of the powerful means frequently utilized in investigating electronic properties of a-semiconductors is the study of their electrical conduction mechanisms. Space charge limited current (SCLC), thermally stimulated current (TSC), thermo-stimulated depolarization (TSD), transient photo-conductivity are amongst the methods employed in electrical conduction analysis of these solids.

Although the scientific understanding of electronic states and conduction mechanisms in a-semiconductors attain remarkably great advancement, there still lacks a closed theorey. Our choise of the samples TNF and Se is multi-fold: Wide field of applications, they can represent large classes of a-semiconductors in their electronic properties, close allignment of electron transport states in a-TNF and Se as evidenced from experiments of photo-injection of charge carriers from a sensitizing layer of a-Se

into TNF[5], lack of datas that are complete and sufficient to understand electronic transport. Thus, this research paper assumed to contribute for the understanding of electrical conduction mechanisms in particular and for the physics of a-semiconductors in general. There by pays its share for sufficient utilization of these and other a-semiconductors for the well being of mankind.

This work devoted in the evaluation of existing theoretical models (for SCLC, TSC and transient photoconductivity) on the basis of experimental observations. Each of the methods considered have their own aspect of preferability in determining specific parameters of traps and charge carrier transport. Hence, more valuable analysis can be made by coordinated utilization of these investigating methods.

In Chapter I, a short review of electronic structure and "native" defect states is presented so as to facilitate the understanding of the core problem. Following is the SCLC theory that costs the entire of Chapter II. In this chapter SCLC analytical I-V characteristic relations will be developed from the stand points of different models. The nature of I-V characteristics predicted by three distribution profiles (discrete, exponential, Gaussian) of traps will be analysed and applicability criterion for these asymptotic I-V relations will be set.

Chapter III gives empahsis on dispersive charge carrier transport properties observed in many a-semiconductors. The physical back ground of this property is illustrated interms of two microscopic mechanisms (hopping and multiple trapping). Quantitative description of these mechanisms will also be considered.

Chapter IV devotes on the theory of thermally stimulated current (TSC). The low temperature ($T < T_g$) TSC spectra and the TSC characteristics around the glass transition temperature T_g will be discussed. In Chapter V experimental details of SCLC, TSC and transient photoconductivity is presented. All the experimental steps, results and analysis of results are included in this chapter. Lastly, conclusion remarks will be presented. The appendix, which consists necessary mathematical formulations, and the biblography are given in the final few pages.

CHAPTER I

A REVIEW OF ELECTRONIC STRUCTURE IN AMORPHOUS SEMICONDUCTORS

Amorphous semiconductors are non-crystalline. The essential difference with respect to their crystalline counter-parts is their lack of long-range order. The short range order being directly responsible for observable semiconductor properties, distinct electrical behaviors in a-semiconductors therefore associated to this lack of long-range ordering.

Understanding of electronic structure is a skeletal base for the subsequent discussions of electrical properties. In this preliminary chapter, general concepts dealing on bonding structure, localized states and "native" defect types are briefly presented.

1.1 Bonding and Structure in A-Semiconductors

Amorphous semiconductors do not consist of close packed atoms. They contain covalentely bonded atoms arranged in an open network with correlations in ordering upto the third or fourth nearest neighbors[6]. On the otherhand, the bonding structure of all covalentely bonded semiconductors is not identical. Some materials such as Ge, Si and others that are formed from compounds of group III and V elements of the periodic table show four-fold coordination (tetrahedrally bonded). In forming the solid, the hybridized orbitals of neighboring atoms will form two new orbitals one of which is a bonding and the other antibonding orbital. Consequently, the wave function delocalization along the bond makes the bonding orbital to occupy the lower energy with respect to the ground state hybridized orbital and the antibonding orbital (largely oscillatory in space) to be raised in

energy by equal amount. Hence, bonding-antibonding energy split.

In contrast to the tetrahedrally bonded, in a great many covalent crystals the hybridization upon formation of the solid consists paired outer orbital electrons that do not involve in bond formation with the neighboring. These are the non-bording or lone-pair electrons. Here bonding is effected only with the remaining two orbitals. For this reason there appears a two-fold coordination. The class of semiconductors sharing the two-fold coordination are mostly refered as chalcogenides. Selenium is an example for this class of semiconductors.

On the basis of the above mentioned facts, customarily semiconductors are classified into two main subfields: Tetrahedrally bonded and chalcogenides. However, there exist also other species exhibiting bonding structure which is bridged between the two major classes. Pincitides are notable groups of semiconductors possesing such feature[7].

Further more, most of the important amorphous solids are molecular solids. On the basis of their network dimensionality, these molecular solids fall into distict catagories. Net-work dimensionality being the number of dimensions in which covalently bonded molecular unit is macroscopically extended[1], the commone solids like sulfur(s), antracene ($C_{14}H_{10}$) for example are zero-dimensional network solids. Selenium (Se) and styrene are on the other hand 1-d. Going to the higher network dimensionality, AS_2S_3 and Ge are typical examples of 2-d and 3-d network solids respectively.

The zero-dimensional network solids molecular units are not macroscopically extended. S_8 and trigonal selenium both being two-fold coordinated

are alike in the extent of their molecular units. Instead of closing back on itself to form a ring the selenium chains keeps on going until terminated by encountering the surface or some other "defect". Solids possesing this feature are called polymers. Figs. 1.1 and 1.2 illustrate the molecular units of trigonal selenium, polystyrene and TNF. In general, polymers differ from other atomic or low molecular weight materials in that they are composed of long chain molecules usually containing a huge number of atoms. As the chemical bonds in these long chain molecules appear no different from those in low molecular weight compounds, it is obvious that the particular properties arise not from the pecularities of chemical bonding but from their long chain nature[10].

As depicted in Figs. 1.1 and 1.2, despite their similarity in forming chains even a relatively simple organic polymer such as polystyrene lacks the ultimate simplicity of polymeric selenium. Because of the bulky side groups (a benzene ring minus one hydrogen) prevent the closure needed to form rings there is apparently no structural complication in organic amorphous solids. (Large rings may be ignored since are very improbable[1]). On the contrary this structural question mark continues to plage amorphous selenium as a result of these closed rings.

Even though the bonding, network dimensionality and extent of molecular units of a solid helps in classifying semiconductors, the characteristic feature being not peculiar to amorphous semiconductors, applied equally for the corresponding crystalline species. This is because of the features underlying the distinction between amorphous semiconductors and their crystalline counterparts are attributed to not the short-range order but the long-range ordering.

1.2 Native Defects and Associated States

Amorphous semiconductors always consist defects. Even when prepared with a large degree of chemical purity they do have a defect. These defects are not of chemical origin resulting from the presence of foreign atoms or molecules. They are associated with the internal conditions of the solid itself. Thus, are called "native" defects[1].

For an ideal crystalline semiconductors, due to the periodicity of atoms solutions of the wave equation provide us density of states having sharp structures consisting of an energy gap completely free of states and bounded by the conduction band edge (Ec) and the valence band edge (Ev). In contrast amorphous solids lack this long-range ordering. Hence, density of states within the gap.

In describing the origin of these defect states, different models have been developed [1,7,8]. In the following few paragraphs a brief explanation of defect states associated with coordination and chain nature is presented.

Electrical, optical and magnetic properties observed in experiments have different characteristics in different classes of a-semiconductors[1,7]. Voids are supposed the single most important defects in teterahedral a-semiconductors. The observed electron-spin-resonance (ESR) signal in these materials is then due to the covalentely unsatisfied bond-prepared orbital projected into the void space. (I.e., due to dangling bonds which remain as unpaired electrons.

For chalcogenides and pnictides the situation is more complex in many ways. As suggested by Kastner[1,7,9], the observed behaviors in chalcogenides are described in terms of spin-paired coordination defects. These defects are designated as C_2°, C_1^- and C_3^+. Where the superscripts and subscripts denote the net charge and covalent coordination respectively (Fig.1.3).

The pairs of charged defects (C^+ and C^-), also called valence alternation pairs (VAPS) can be formed by the transfer of an electron from one dangling bond to another. The charge-transfer bond switching reaction is expressed as

$$2\ C_2^{\circ} \rightarrow C_3^+ + C_1^- \qquad (1.1)$$

Eq.1.1 describes the creation of VAPS from a fully bonded network in which all atoms are in the C_2° configuration. The energy needed to convert a pair of chain ends into a VAP is an effective correlation energy Ueff. The energy Ueff is negative and is in agreement with that required by Anderson[1]. The existence of the spin-paired charged defect states is related in an intimate way to the non-bonding or lone-pair electrons.

Analogously the charged defect states in pnictides would be labelled P_2^- and P_4^+. In a-semiconductors with both group V and VI atoms present, a larger number of coordination-type defect pairs are possible[9].

A number of works performed on polymeric semiconductors indicate the existence of other possible defect types. These are associated to chain distortions[10-13]. The essentially two-fold coordination found in semiconducting polymers makes these systems generally more succeptible to

structural distortions than in the case with the usual tetrahedral semiconductors. The anticipation, that the type of defect of interest is a "soliton" defect[13,14]. Associated with each soliton is an energy level at midgap. The soliton and its associated pair (antisoliton) may not separate far upon their formation. Then, two soliton wave functions can be combined together to make new energy levels and new particles (polarons). Thus, polarons viewed as a localized distortion of bonds within a uniform bond alternation pattern. Further more, if the soliton and the antisoliton comprising the polaron are both charged, there can result a further distortion of the local bonding pattern, forming a bipolaron. In summary, the defect states of major importance in polymeric a-semiconductors are ought to be the solitons, polarons and bipolarons. The charge 1 spin relation of polarons and bipolarons depicted in table 1.1 provides a clue for observed electrical and magnetic properties.

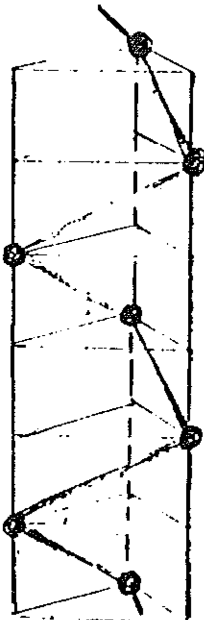

Fig 1.1: Asingle polymer chain in trigonal selenium.

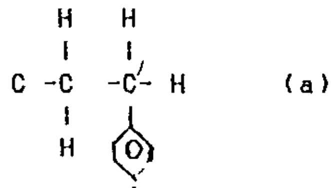

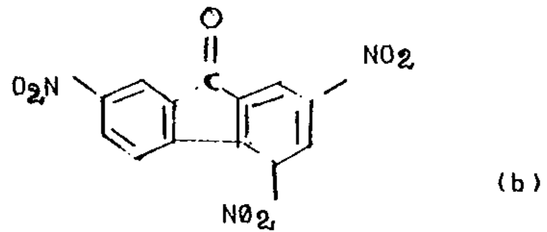

Fig 1.2: Structural formulas of plysterene(a) and trinitro-nine-flourenone (b)

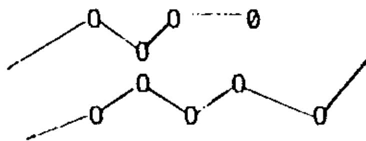

(a) Idealized bonding

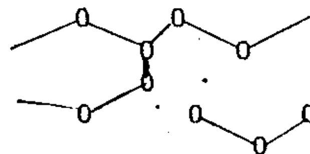

(b) Valance-alternation pair

Fig 1.3: Valance-alternation defects in a network based on two-fold coordinated atoms.

Table 1.1
Charge/spin relation of polarons(P) and bipolarons(BP)

Defect type	Net charge	Spin
P^+	+1	1/2
P^-	-1	1/2
BP^{++}	+2	0
BP^{--}	-2	0

CHAPTER II

STEADY STATE SPACE CHARGE LIMITED CURRENT

Analysis of space charge limited current (SCLC) have been widely used as an effective means for the study of parameters that characterize localized states influencing electrical conduction in solids[15-19]. Charge carriers injected into the specimen from metal electrode forming ohmic contact with it, get immobilized by traps situated in the mobility gap. Thus, influnce of traps on the actual forms of I-V characteristics and physical basis for the application of SCLC study.

The general scheme of SCLC experimental arrangement is as depicted in Fig.5.1. Electrons (or holes for hole injecting contact) injected from the cathode ($X=0$). The role of the anode being as a collector for electrons arriving at $X=L$ (L is electrode-electrode spacing). The blasing voltage realized by external circuit make the injected carriers sweep across the sample towards the anode. The aim of the chapter is then to develop and value relations describing the nature of electrical conduction under this experimental condition.

2.1 Analytical Equations for SCLC

The main task here is to solve the current flow equation together with Poisson's equation on the basis of the following simplifying assumptions:

- Diffusion currents are neglected.
- A plane-parallel sample of uniform dielectric is considered. Density of traps and mobility of charge carriers are taken to be constant through the sample.

- The cathode is taken as the infinite reservoir of carriers available for injection at X=0, the counter electrode being at X=L.
- Quasi-equilibrium condition, thus quasi-steadystate Fermi-level concept assumed valid.

Basic equations to be solved are:

$$J(x) = e_o \mu n (x)F(x) \tag{2.1}$$

$$\frac{\varepsilon}{e_o} \frac{\partial}{\partial x} F(x) = n_c(x) + n_t(x) \tag{2.2}$$

$$F(x) = - \frac{\partial V(x)}{\partial X} \tag{2.3}$$

The density of free electrons $n_c(x)$ and concentration of electrons trapped by localized states situated between energies E_1 and E_2 can be put respectively as

$$n_c(x) = N_c \, e^{\frac{-(E_c-E_F)}{KT}} \tag{2.4}$$

$$n_t(x) = \int_{E_1}^{E_2} f(E)g(E)dE \tag{2.5}$$

The meanings of the symbols used are summerized as follows; e_o=-electronic charge, μ=-drift mobility of carriers, ε_r=-dielectric constant ($\varepsilon = \varepsilon_r \, \varepsilon_o$) and ε_o is permitivity of free space, J(x)=-current density, F(x) and V(x) are electric field and potential difference respectively, N_c is concentration of available states in the conduction band, E_C and E_F are the magnitudes of energy corresponding to the lower edge of the conduction band and the Fermi energy respectively, K is the Boltzman's constant, T is the temperature in Kelvin, g(E) and f(E) are the energy distribution of traps and the Fermi-Dirac functions respectively.

$$f(E) = \frac{1}{1+e^{(E-E_F)/KT}} \qquad (2.5')$$

Boundary conditions we need in solving the above set of equations on the basis of the adopted assumptions are

$$\begin{aligned} n\ (x = 0) &= 0 \\ F\ (x = 0) &= 0 \end{aligned} \qquad (2.6)$$

We require to calculate anodic values of measurable quantities. Thus, free and trapped electron concentrations at the anode being denoted by n_{cL} and n_{tL} respectively, eq.2.2 can be rewritten as[18].

$$\frac{\varepsilon}{e_o} k_2 \frac{F(L)}{L} = n_{cL} + n_{tL} \qquad (2.7)$$

i.e.,

$$\frac{\varepsilon}{e_o} \kappa_1 \kappa_2 \ V/L^2 = n_{cL} + n_{tL} \qquad (2.8)$$

where

$$\tfrac{1}{2} \leq \kappa_2 \leq 1 \quad \text{and} \quad 1 \leq \kappa_1 \leq 2 \qquad (2.9)$$

For low applied voltage, the current in the sample will obey Ohm's relation. Therefore by eq.2.1

$$J(L) = e_o \mu k_1 n_o \ V/L \qquad (2.10)$$

where n_0 is the initial thermal equilibrium free electron concentration. This is a reasonable approximation since the density of injected electrons is very much less than the initial thermal equilibrium value for a sufficiently low voltage.

For increased P.d, probability of injection of excess charge into the sample will increase. As a result, departure from Ohm(s law hence SCL conduction follows. Injected carriers since partly contribute to filling of traps and partly to free carrier concentration, by virtue of Eq.2.5, SCLC characteristics practically depend on the nature of energy distribution of traps. In the present we emphasize the case for three typical distribution profiles. These are:

Mono-energetic $$g(E) = N_t \delta (E-E_t) \quad (2.11)$$

Exponential $$g(E) = \frac{N_t}{2s} e^{-|E-E_t|/s} \quad (2.12)$$

Gaussian $$g(E) = \frac{N_t}{\sqrt{2\pi}\sigma} e^{-\frac{(E-E_t)^2}{2\sigma^2}} \quad (2.13)$$

where sand σ are distribution parameters for the exponential and Gaussian energy profiles of traps respectively and E_t it the energy at which a given distribution is centered. N_t is the total concentration of traps.

a) Mono-Energetic Traps

In the situation where traps are populated at a single energy level, Eq.2.5 gives

$$n_{tL} = \frac{N_t}{1+e^{(E_t-E_F)/KT}} \quad (2.14)$$

Using Eq.2.4 this will yield

$$n_{tL} = \frac{N_t}{1+\frac{N_c}{n_{cL}} e^{-E_t'/KT}} \quad (2.15)$$

Where E_t' is energy depth of traps measured from the lower edge of conduction band. Substituting Eq.2.15 in 2.7 and using Eq.2.8

$$\frac{\varepsilon}{e_o} k_1 k_2 V/L^2 = n_{cL} + \frac{N_t}{1+\frac{N_c}{n_{cL}} e^{-E_t'/KT}} \tag{2.16}$$

At elevated injection level the greatest portion of injected charge carriers go in trap filling process. Therefore, from the approximation in Appendix A, the anodic value of the current density will be

$$J(L) = \varepsilon \mu k_1^2 k_2 \ V^2/L^3 \ (\frac{N_t}{N_t}) \ e^{-E_t'/KT} \tag{2.17}$$

When the injection level surpasses the traps energy, the mode of conduction will be non trap-limited. The second term in Eq.2.16 therefore can be neglected. As a result the current density for injection level above trap saturation will have the form

$$J(L) = \varepsilon\mu k_1^2 k_2 \ V^2/L^3 \tag{2.18}$$

This is a trap free SCLC density. It is identical with SCLC of semiconductors without traps. One can obtain J-V relations for higher order discrete energy levels by using the same principle.

b) Exponential Distribution

The exponential distribution we shall consider is a double-exponential distribution (Eq.2.12). For traps distribution centered at the mobility edges (E_C or E_V), this will be reduced to semi-infinite exponential form. To develop quantitative J-V expressions for trap controlled SCLC, we consider Eq.2.5. Using Eq.2.12 this results

$$n_{tL} = \frac{N_t}{2S} \int_{E_1}^{E_2} \frac{e^{-(E-E_t)/S}}{1+e^{(E-E_F)/KT}} dE \qquad (2.19a)$$

When the applied voltage is such that E scans the lower portion of the distribution, Eq.2.19a will give

$$n_{tL} = \frac{N}{2S} \int_{E_L}^{E_t} \frac{e^{-(E_t-E)/S}}{1+e^{(E-E_F)/KT}} dE \qquad (2.19b)$$

where E_L is the lower energy in the distribution. Defining $S=KT_c$, T_c be characteristic temperature of the distribution, we will obtain

$$n_{tL} = \frac{N_t}{2KTr} \int_{E_L}^{E_t} \frac{e^{-(E_t-E)KTr}}{1+e^{(E-E_F)/KT}} dE \qquad (2.20)$$

and r is defined by $r=T_c/T$. Using the arguement leading to Eq.A3. one can get

$$n_{tL} = \frac{N_t}{2KTr} \int_{E_L}^{E_t} e^{-\left(\frac{E_t-E}{KTr}\right)} \quad e^{-\left(\frac{E-E_F}{KT}\right)} \quad dE \qquad (2.21)$$

whence

$$n_{tL} = \frac{N_t}{2(r-1)} \frac{n_{cL}}{N_c} e^{(E_t'-E_L')/KTr} \quad e^{\frac{E_L'}{KT}} \qquad (2.22)$$

Then from A6

$$n_{cL} = \frac{\varepsilon}{e_o} k_1 k_2 2(r-1) \frac{N_c}{N_t} \frac{V}{L^2} e^{\frac{(E_L'-E_t')}{KTr}} \quad e^{-E_L'/KT} \qquad (2.23)$$

Thus,

$$J = \varepsilon\mu k_1^2 k_2^2 2(r-1)\frac{N_c}{N_t} \frac{V^2}{L^3} e^{\frac{(E_L'-E_t')}{KTr}} \quad e^{-E_L'/KT} \quad E_L < E_F < E_t. \qquad (2.24)$$

When the quasi Fermi level lies above E_t, trapped carriers density is calculated by considering the trap occupancy from lower edge of the distribution up to E_F.

Hence,

$$n_{tL} = \frac{N_t}{2KTr} \int_{E_L}^{E_F} \frac{e^{-(E-E_t)/KTr}}{1+e^{(E-E_F)/KT}} \, dE \quad (2.25)$$

$$n_{tL} = \frac{N_t}{2} \left\{ \int_{-\omega_L}^{o} \frac{e^{\omega}}{1+e^{\omega r+y}} - \int_{o}^{\omega' s} \frac{e^{-\omega'}}{1+e^{-r\omega'+y}} \, d\omega' \right. \quad (2.26)$$

where

$$\omega = \frac{E-E_t}{KTr}, \quad \omega_L = \frac{E_t-E_L}{KTr}, \quad \omega' = \frac{E_t-E}{KTr}, \quad \omega_F' = \frac{E_t-E_F}{KTr} \text{ and } Y = \frac{E_t-E_F}{KT}$$

For injection level of such order, the exponential terms in the denominators of the above integral equations can be neglected. Solving for n_{tL} with such an approximation results

$$n_{tL} = \frac{N_t}{2} \, e^{(E_F-E_t)/KTr} \quad (2.27)$$

Combining this with Eqs.2.4 and 2.8 yields

$$n_{cL} = \left(\frac{2\varepsilon_1 k_1 k_2}{e_o N_t}\right)^r n_c \frac{V^r}{L^{2r}} \, e^{-E_t'/KT} \quad (2.28)$$

Therefore, the current density will be

$$J(L) = e_o^{1-r} \, \mu \, k_1 \left(\frac{2\varepsilon k_1 k_2}{N_t}\right)^r \frac{V^{r+1}}{L^{2r+1}} \, N_c \, e^{-E_t'/KT} \quad (2.29)$$

For an injection level exceeding the trap filled limit, the resulting current density can equivalently be described by Eq.2.18.

c) Gaussian Distribution

The other distribution profile of traps adopted in describing experimental results of SCL conduction is the Gaussian distribution (Eq.2.13). For an injection level at which E_F lies below E_{t_1}, from Eqs.2.5 and 2.13 we will have

$$n_{tL} = \frac{N_t}{\sigma\sqrt{2\pi}} \int_{E_1}^{E_t} \frac{e^{-\frac{(E-E_t)^2}{2\pi^2}}}{1+e^{(E-E_F)/KT}} \, dE \tag{2.30}$$

$$n_{tL} = \frac{N_t}{\sqrt{2\pi}} \int_{o}^{Y_1} \frac{e^{-y^2/2}}{1+e^{1/KT(x-\sigma y)}} \, dY \tag{2.31}$$

where

$$Y = \frac{E_t - E}{\sigma}, \qquad X = E_t - E_F, \quad Y_1 = \frac{E_t - E_1}{\sigma\sqrt{2}}$$

When the injection level scans the lower "tail" of the distribution, from B_6 we have

$$n_{cL} = \frac{\varepsilon}{e_o} k_1 k_2 \frac{V}{L^2} \; e^{-1/KT(E_t^{'} + \sigma^2/2KT)} \tag{2.32}$$

Then,

$$J(L) = \varepsilon \mu \, k_1^2 k_2 \frac{N_c}{N_t} \frac{V}{L^3} \; e^{-1/KT(E_t^{'} + \sigma^2/2KT)} \tag{2.33}$$

for

$$E_F < E_t - \frac{\sigma^2}{2KT}$$

In a subsequent increase of injection level, E_F traverses the steep

portion of the distribution below E_t. Thus, for $E_t - \frac{\sigma^2}{KT} < E_F < E_t$, Eq.2.31 calculated to give (B 18)

$$n_{cL} = N_c\, e^{-E_t'/KT + 2} \quad e^{-1/KT \sqrt{2\sigma^2[1+(\frac{2KT}{\sigma})^2] \quad \ell_n(\frac{e_o L^2 A}{\varepsilon k_1 k_2 V})}} \qquad (2.34)$$

The current density is therefore given by

$$J(L) = e_o\, \mu\, k_1 N_c (V/L) e^{-E_t'/KT+2} \quad e^{-1/KT \sqrt{2\sigma^2[1+(\frac{2KT}{\sigma})^2] \quad \ell_n(\frac{e_o L^2 A}{\varepsilon k_1 k_2 V})}} \qquad (2.35)$$

Further increase of applied voltage through a medium high voltage region up to V_{TFL} (trap filled limit voltage), demand the trap occupancy to be written as

$$n_{tL} = \frac{N_t}{\sigma\sqrt{2\pi}} \int_{E_1}^{E_{TFL}} \frac{e^{-(E-E_t)^2/2\sigma^2}}{1+e^{(E-E_F)/KT}}\, dE \qquad (2.36)$$

Following the arguments made in former sections, the limits of the integral can be taken to be infinity. This is reasonable approximation as far as a relatively small dispersion parameter σ is taken into account. With this

$$n_{tL} = \frac{N_t}{\sqrt{\pi}} \int_{-\infty}^{\infty} \frac{e^{-Y^2}}{1+e^{1/KT(-X+\sqrt{2}\sigma y)}}\, dY \qquad (2.37)$$

where

$$Y = \frac{E-E_t}{\sigma\sqrt{2}} \quad \text{and} \quad X = E_F - E_t$$

From B37 (integral in Eq.2.37 evaluated in Appendix B)

$$n_{tL} = \frac{N_t}{1+e^{(E_t-E_F)/KT\ell}} \qquad (2.38)$$

Where

$$\ell = \sqrt{1 + \frac{2\pi\sigma^2}{16K^2T^2}} \qquad (2.39)$$

Eq.2.38 equivalentely be written as (using Eq.2.4)

$$n_{tL} = \frac{N_t}{1+(N_c/n_{cL}\ e^{-E_t'/KT})^{\ell}} \qquad (2.40)$$

The voltage corresponding to trap filled value is (by Eq.2.8)

$$V_{TFL} = \frac{e_o L^2 N}{\varepsilon k_1 k_2} \qquad (2.41)$$

On the other hand

$$V = \frac{e_o L^2}{\varepsilon k_1 k_2} \{n_{cL} + n_{tL}\} \qquad (2.42)$$

For $V < V_{TFL}$, from Eqs. 2.41 and 2.42

$$\frac{V_{TFL}}{V} \doteq 1 + (\frac{N_c}{n_{cL}}\ e^{-E_t'/KT})^{1/\ell} \qquad (2.43)$$

(Since n_{cL} is sufficiently less than N_t). Therefore, Eq.2.43 when solved for n_{cL} yields

$$n_{cL} = \frac{N_c\ V^{\ell}}{(V_{TFL} - V)^{\ell}}\ e^{-E_t'/KT} \qquad (2.44)$$

Hence,

$$J(L) = e_o \mu k_1 N_c \frac{V^{\ell+1}}{L} \frac{e^{-E_t^{'}/KT}}{(V_{TFL} - V)^{\ell}} \tag{2.45}$$

In the situation when V exceeds V_{TFL}, from Eqs.2.40 and 2.42

$$V' = \frac{e_o L^2}{\epsilon k_1 k_2} \{ n_{cL} + \frac{N_t}{1+(\frac{N_c}{n_{cL}} e^{-E_t^{'}/KT})^{1/\ell}} \} \tag{2.46}$$

The current density in trap free SCL flow can therefore be expressed by

$$J(L) = e_o \mu k_1 n_{cL} V'/L \tag{2.47}$$

In this last step the current density tend to exhibit a power dependence (on V) greater than order of three ingeneral.

2.2 Applicability of SCLC Analytical Equations

The functional forms of the set of J-V characteristic approximations gears us to value their respective behavior under certain changes of experimentally controllable (or measurable) parameters such as V,T,L. The nature of asymptotic SCLC equations in regard to their dependence either on the applied potential or temperature while other parameters kept fixed is depicted in table 2.1.

Table 2.1

$m = \frac{d\log S}{d\log V}$ and $n = \frac{d\log S}{d(YT)}$ behavior

Characteristics	Mono energetic	Exponential distribution	Gaussian distribution
logj Vs logV	linear m=constant	linear m=constant	non-linear m≠constant
logj Vs 1/T	linear n=constant	linear n=constant	non-linear n≠constant

Figs.2.1 and 2.2 illustrate the non-linear dependence of SCLC with temperature. The graphs represent simulated behavior of asymptotic SCLC characteristics for traps assumed to have Gaussian distribution profile. Fig.2.1 demonstrates the feature when the distribution centered at the mobility edge (ge(E) type distribution). Fig.2.2 on the other hand is for a distribution centered within the mobility gap (ge(E) type distribution). The characteristic difference between the two Gaussian distribution, in regard to their temperature sensitivity is summarized in table 2.2.

In practice, comparison of experimental curves with the simulated graphs on the basis of certain priorily assumed distribution profile may speak infavour of a distribution found to describe observed SCLC characteristics. Ruling out of the distributions not sharing common feature with observable characteristics is guaranted at this stage.

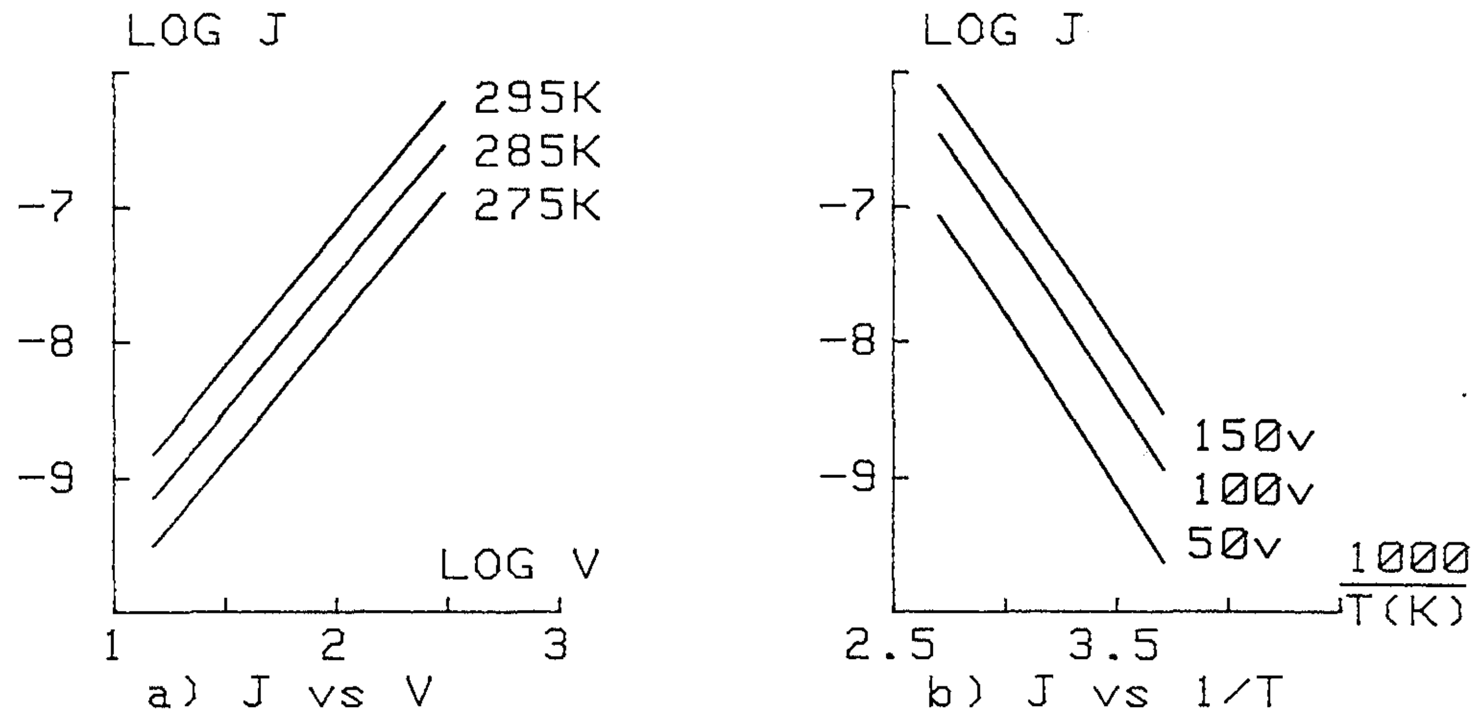

Fig 2.1: Temperature dependence of SCLC for $g_g(E)$ distribution. $Nc=1\times10^{21}$ (cm-3), $Nt=2\times10^{17}$ (cm-3) Et=.29, s=.08ev, L=300um.

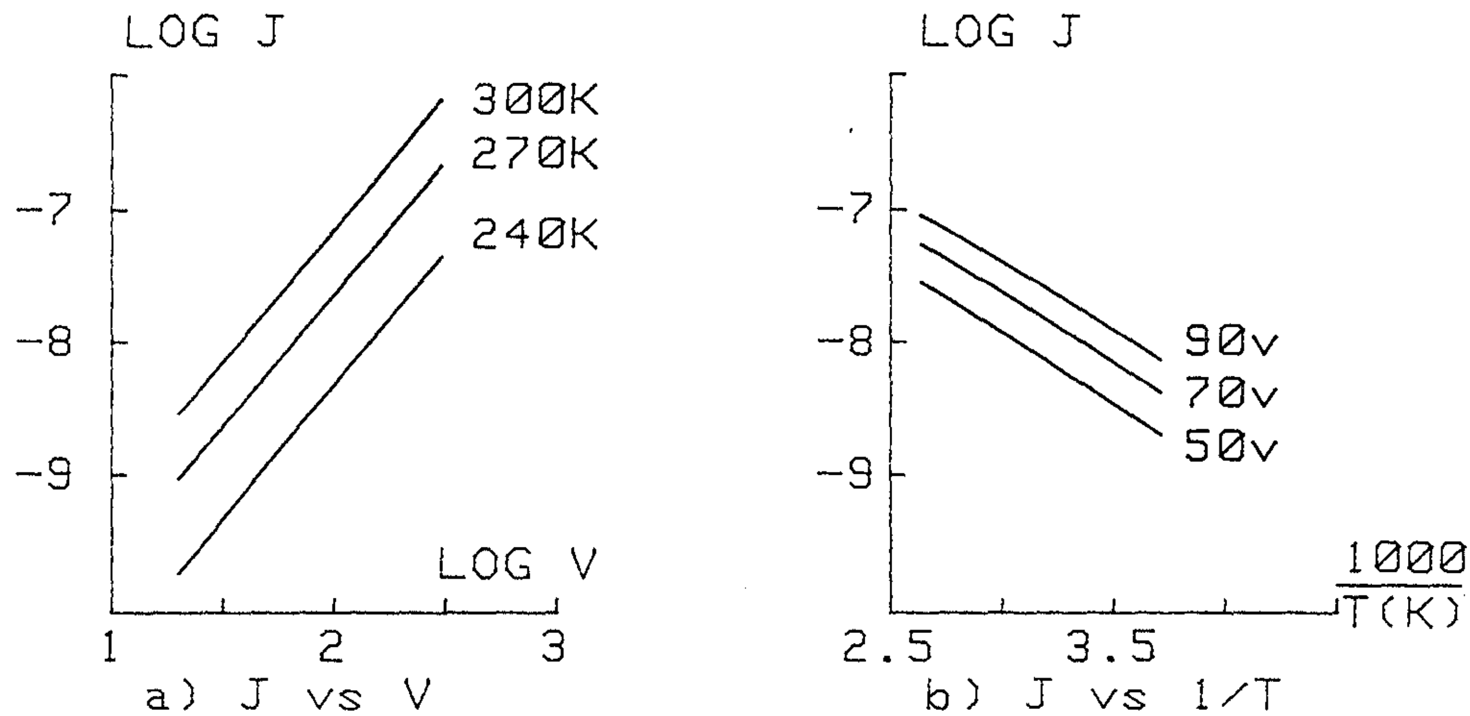

Fig 2.2: Temperature dependence of SCLC for $g_c(E)$ distribution. $Nc=1\times10^{21}$ (cm-3), $Nt=2\times10^{17}$ (cm-3) Et=0, s=.08ev, L=300um.

Table 2.2

Characteristic differences between $g_e(E)$ and $g_g(E)$ on the nature of their SCLC

Characteristics	$g_e(E)$	$g_g(E)$
logj Vs log V	m increases with decreasing T and J-V converge at the "half filled" Gaussian "bell" limit.	Increase of m with T is less pronounced and J-V converge as $V \longrightarrow V_{TFL}$
Logj Vs Yt	Slope(n) decreases as V increases.	Slope remains practically parallel.

CHAPTER III

DESPERSIVE TRANSPORT IN AMORPHOUS SEMICONDUCTORS

Observation of the time dependence of current in many a-semiconductors in a small signal condition shows a dispersive character. For normal transport process in crystalline materials, time evolution of the current posseses a definite transit time (Fig.3.1). In the amorphous counter parts, the current pulse observed during transient photoconductivity experiments [20-22] (identical to that in Fig.5.5) exhibit featurless behavior with no identifiable transit time (Fig.3.2). Furthermore, charge carrier drift mobility, μ, in a-semiconductors found to be dependent on extrinsic parameters such as; applied field, sample thickness, and temperature[20, 23,24]. This chapter will devote to the theories of dispersive transport property in a-semiconductors.

3.1 Microscopic Mechanisms Underlying Dispersive Transport

Anomalous I(t) behavior observed following a short pulse photo excitation of carriers in a-semiconductors is due to the effects of localized states in charge carriers transport process. For an explantion of the way localized states take part in the conduction process hence for the physical orgin of dispersive transport property in these materials two microscopic mechanisms have been set as candidates[20,24,25]. These are demonstrated by energy level diagram of Fig.3.3.

Mechanisms indicated by I and II represent the interruption of extended state carrier transport by trapping events. This is known as multiple trapping. The role of localized states here is to impede transport: i.e. it

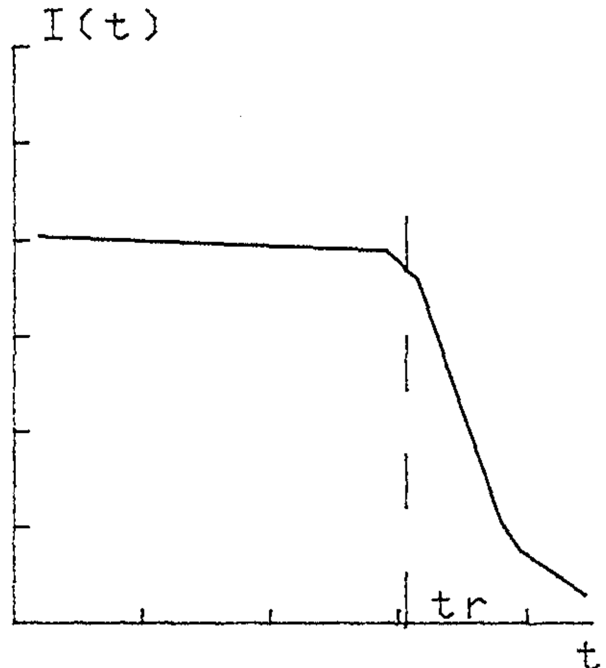

Fig 3.1:Transient current in normal transport

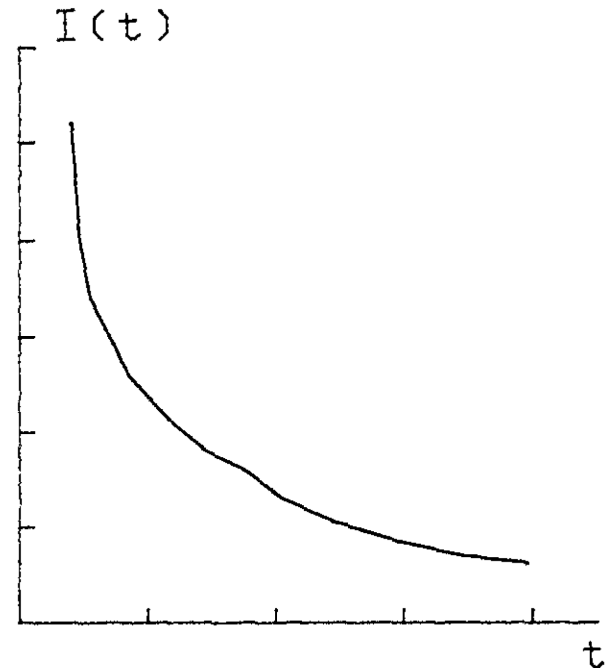

Fig 3.2:Transient current in dispersive tr-ansport

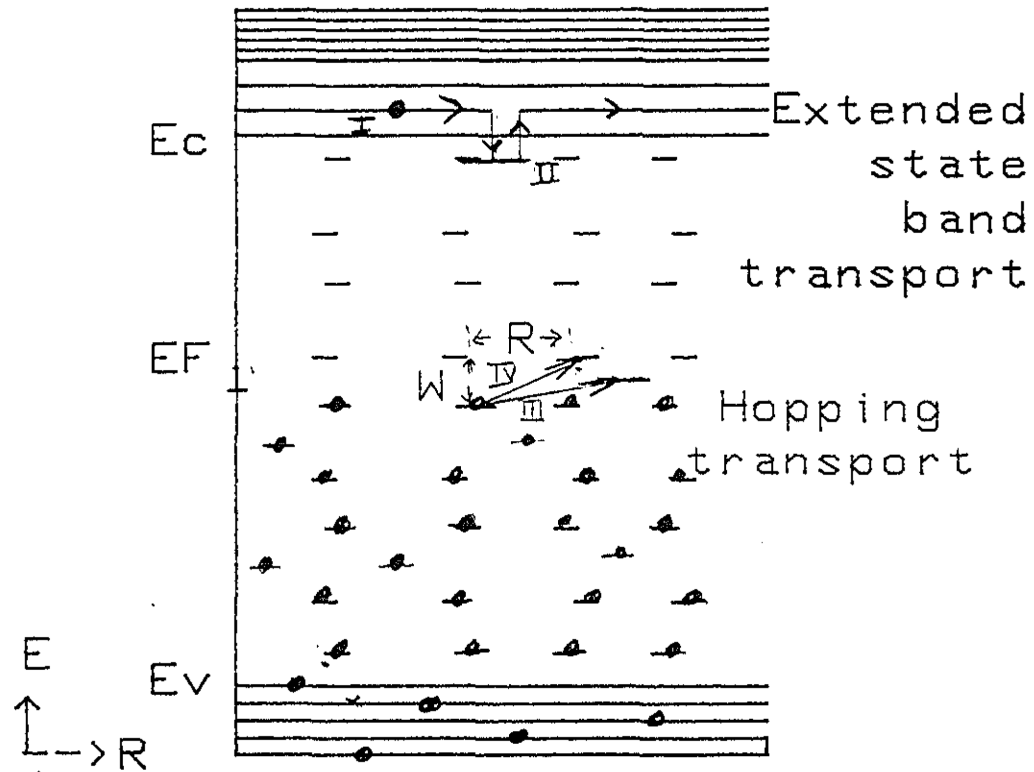

Fig 3.3 : Energy diagram for illustrating conduction mechanism in a-semiconductors

corresponds to a sequence of release of carriers from one site followed by trapping at a second site. The release time, is not in general uniform. Rather, has a broad distribution since release rate decays exponentially with energy depth of traps relative to the conduction edge E_C. One can thus, invisage how this mode of conduction can provide a means to test distribution profile of traps.

The second mechanisms (III and IV in Fig.3.3) in general consists the transfer of electrons from one localized state to the other via direct quantum mechanical tunneling. In conduction realized by hopping between localized states, the temperature independent hopping distance R is assumed to vary stochastically in the system. The reason that such a fluctuation can cause strong dispersion is directly seen from the expression which relate this hopping distance to the hopping probability, P[22, 25,26].

$$P = \nu ph \; e^{-2\alpha R} \; e^{-W/KT} \qquad (3.1)$$

Where νph is the phonon frequency. It follows that hopping mobility μ_L is expected to be of the form[21,26]

$$\mu_L = \mu_o \; e^{-W/KT} \qquad (3.2)$$

The applicability of Eqs.3.1 and 3.2 is indoubt at low temperatures for those localized states near E_F. As the temperature is lowered, the number and energy of phonons decrease and the more energetic phonon-assisted hops will progressively become less favorable. Carriers will tend to hop to larger distances in order to find states which lie energe-

tically closer than the nearest neighbors. This mechanism is known as variable range hopping. In this situation the hopping mobility obeys[25]

$$\mu = \mu_o e^{-C/T^{1/4}}$$

The numerical factor C in general is functions of intrinsic parameters of localized states.

Suspending the more detailed treatment for the next section we shall put the following note for the present: Despite their distinct nature, it is rather difficult to distinguish between the two mechanisms soley on the basis of experiment. But there is a common belief that hopping to be responsible for dispersive transport in certain molecularly doped organic poymers and mutlipple trapping in chalcogenides[1,7].

3.2 Hopping Conduction

Dispersive transport theory developed by M. Seher and E.W. Montroll[20] describes the dynamics of a carrier packet excuting a time dependent random walk in the presence of field dependence spatial bias and an absorbing barrier at the sample surface. A brief account of this model is considered next.

Following this theory, we consider the sample to be subdivided into a regular lattice of equivalent cells with each cell containing many randomly distributed sites available for hopping carriers. The hopping time being defined to be the time interval between the moment of arrival of a carrier into one cell and the moment of arrival into the next cell

into which it lands, the temporal aspect is said to be governed by an event time distribution, $\psi(t)$. Therefore, the random distribution of sites and hence disorder of the material is incorporated to $\psi(t)$.

In this stochastic model the basic quantity of the theory is, the probability that a walker is found at ℓ a time t if at the initial time ($t = o$) it was at the origin: i.e $\bar{G}(\ell,t)$. The hopping time distribution $\psi(t)$ and $\bar{G}(\ell,t)$ are related as[20].

$$\bar{G}(\ell,t) = \frac{1}{2\pi i} \int_{c-i\infty}^{c+\infty} e^{st} [1-\psi^*(S)] G(\ell,\psi^*(S)) \frac{dS}{S} \tag{3.4}$$

where

$$\psi^*(S) = L\{\psi(t)\} \tag{3.5a}$$

(i.e $\psi^*(S)$ is Laplace transform of $\psi(t)$)

and $G(\ell,y)$ is a random-walk generating function. For periodic boundary conditions $G(\ell,y)$ can be put as

$$G(\ell,y) = \prod_{j=1}^{3} \frac{1}{N_j} \sum_{m_1,m_2,m_3=1} \frac{e^{i\vec{\ell}.\vec{k}}}{1-y\Lambda(k)} \tag{3.6}$$

$$k_j = \frac{2\pi m_j}{N_j} \quad \text{where } \vec{k} \text{ is a wave vector}$$

The quantity $\Lambda(k)$ is related with the transition probability of hops from one cell to the other displaced by $\vec{\ell}$ from it through Fourier representation as

$$\Lambda(k) = \sum_{\ell} P(\ell) e^{-i\vec{\ell}.\vec{k}} \tag{3.7}$$

Assuming the spatial biasing field to be in the x direction (ℓ_1 direction), the mean of the carrier packet will be

$$\langle \ell \rangle = \langle \ell_1 \rangle \equiv \sum_{\ell} \ell_1 \bar{G}(\ell_1 t) \tag{3.8}$$

Knowing $\langle \ell \rangle$, the carrier current can be computed using the relation

$$I(t) \propto \frac{d\langle \ell \rangle}{dt} \tag{3.9}$$

Our next task is to solve Eq.(3.9) for typical hopping time distribution $\psi(t)$. A calss of hopping time distribution functions that are consistent with observations are those forms of $\psi(t)$ with long tails which decay asymptotically as $t \to \infty$. Mathematical generalization of these class of functions is[20]

$$\psi^*(t) \sim Ct^{-(1+\alpha)}/\Gamma(1-\alpha) \quad 0 < \alpha < 1 \tag{3.10}$$

From Eq.3.5a

$$\psi^*(S) = \int_0^\infty e^{-st}\, \psi(t)dt \qquad (3.5b)$$

Taking the Taylor series expansion of e^{-st}, this can be put as

$$\psi^*(S) \approx 1 - S\bar{t} + \tfrac{1}{2} S^2 \langle t^2 \rangle$$

where $\bar{t} = \langle t \rangle$ and $\langle t^n \rangle = \int_0^\infty t^n \psi(t)dt.$

We need to utilize the following Tauberian theorm for the calculation[27].

If $L\{f(t)\} \sim AS^{-\beta}$ as $s \to 0$ with $\beta > 0$ then

$$f(t) \sim At^{\beta-1}/\Gamma(\beta) \quad \text{as} \quad t \to \infty \tag{3.13}$$

Where f(t) is a function of the variable t.

Hence, by Eq.3.13 one will get (Appendix C)

$$\psi^*(S) = 1-CS^{\alpha} \equiv 1-S^{\alpha}/A \qquad (3.5c)$$

$$A = C^{-1}$$

If we now consider the Fourier component of $\bar{G}(\ell,t)$, i.e.,

$$\gamma(k,t) = \sum_{\ell} \bar{G}(\ell,t)e^{-(\vec{k}.\vec{\ell})} \qquad (3.14)$$

and use Eqs.3.4 and 3.6, we obtain

$$\gamma(k,t) = L^{-1}\{(1-\psi^*(S))[S(1-\Lambda(k))\psi^*(S)]^{-1}\} \qquad (3.15)$$

Therefore, by Eq.3.8 mean position of the carrier packet will have the form

$$\langle \ell_1(t) \rangle = \bar{\ell}\left(\frac{\partial\gamma}{\partial\Lambda}(k,t)\right)_{\Lambda=1} \qquad (3.16)$$

Where

$$\bar{\ell} = \Sigma \ell P(\ell) \qquad (3.17)$$

Thus, by Eq.3.15; $\langle \ell_1(t) \rangle = \bar{\ell}\, L^{-1}\{\psi^*(S)/S(1-\psi^*(S))\}$ (3.18)

Consequently, using Eq.3.14 one will find the functional form of $\langle \ell_1(t) \rangle$ to be

$$\langle \ell_1(t) \rangle \sim \bar{\ell}\, At^{\alpha}/\Gamma(1+\alpha) \qquad (3.19)$$

If similar technique is employed to compute for D, using the relation

$$D^2 = \langle (\ell - \langle \ell \rangle)^2 \rangle \qquad (3.20)$$

then, the dispersion to mean ratio will be found to behave as

$$\frac{D}{\langle \ell \rangle} \sim \{ [2\,\Gamma^2(1+\alpha)/\Gamma(1+2\alpha)]-1 \}^{\frac{1}{2}} \tag{3.21}$$

The result in Eq.3.21 shows $D/\langle \ell \rangle$ is independent of time. The physical explanation of this is illustrated in Fig.3.4. When inverse power tail (Eq.3.10) exists, contrary to Gaussian packet (whose peak and mean carrier packet are located at the same position and move with the same velocity as in Fig.3.4a), the mean carrier packet propagates with a velocity which decrease with time as it separates from the peak which remains nearly fixed at the point of creation of carriers (Fig.3.4b). From Eqs. 3.9 and 3.19

$$I(t) \sim \bar{\ell}\, A t^{-(1-\alpha)}/\Gamma(1+\alpha) \qquad 0<\alpha<1 \tag{3.22}$$

The hopping time distribution and consequently the associated current in Eq.3.22 do not take into account the eventual arrival of carriers at the back electrode $(x = L)$ at which they dissapear. With such effect of the absorbing boundary at the sample back surface, let us consider the Fourier component of $\bar{P}(\ell,t)$: the probability for a carrier starting at origin at $t = o$, to be found at ℓ at time t, expressed as

$$\bar{P}(\ell,t) = \bar{G}(\ell-\ell_o,t) - \int_o^t \bar{G}(\ell,t-t')\,\bar{F}(L-\ell_o,t')dt' \tag{3.23}$$

Here, $\bar{F}(\ell,t)$ is the first passage-time distribution function for the transition $\ell_o \to L$. $\bar{G}(\ell-\ell_o,t)$ is the unperturbed propagator for the transition $\ell_o \to \ell$. Then

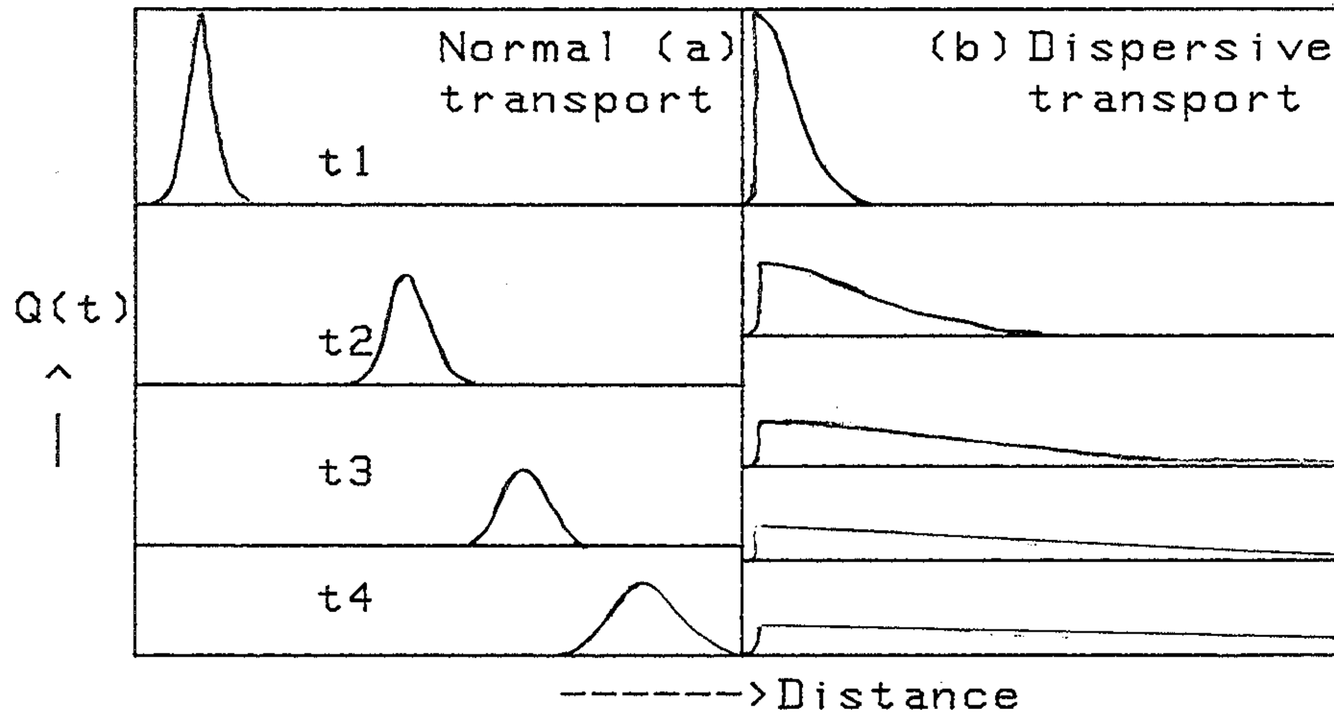

Fig 3.4: Time evolution of the carrier-density Q(t) profile of the injected charge pulse.

$$\Gamma(k,t) = \gamma(k,t)\, e^{-ik\ell_o} - \int_o^t \gamma(k,t-t')\bar{F}(L-\ell_o,t')dt' \qquad (3.24)$$

Proceeding in the same manner as the infinite sample case, one will reach at the relation

$$\langle \ell \rangle = i \lim_{k \to o} \frac{\partial \Gamma^{(k,t)}}{\partial k} \qquad (3.25)$$

The mean position of the propagating packet then calculated to be

$$\langle \ell \rangle \sim \ell_o + \bar{\ell}AC - \bar{\ell}\beta\, t^{-\alpha}/\Gamma(1+\alpha) \qquad (3.26)$$

Therefore,

$$I(t) \sim \frac{d\langle\ell\rangle}{dt} \sim \beta\bar{\ell}\, t^{-(1+\alpha)}/\Gamma(\alpha) \qquad (3.27)$$

Inclusion of the effect of absorbing electrode then adds further decrease of the current with time. Eq.3.27 is the asymptotic behavior of I(t) for times long enough so that $\langle\ell\rangle \gg L$. Thus, the overall behavior of the photo-induced transient current will have the general form

$$I(t) \sim t^{-(1-\alpha)} \qquad t < t_r \qquad (3.28)$$

$$I(t) \sim t^{-(1+\alpha)} \qquad t > t_r \qquad (3.29)$$

This is illustrated schematically in Fig.3.1. The photoinduced current shows a change in its time dependence from a power of $-(1-\alpha)$ to $-(1+\alpha)$ at a transit time t_r which can clearly be seen in a log-log plot of Fig.3.5. This feature infact not found on the apparent I(t) V_s t plot.

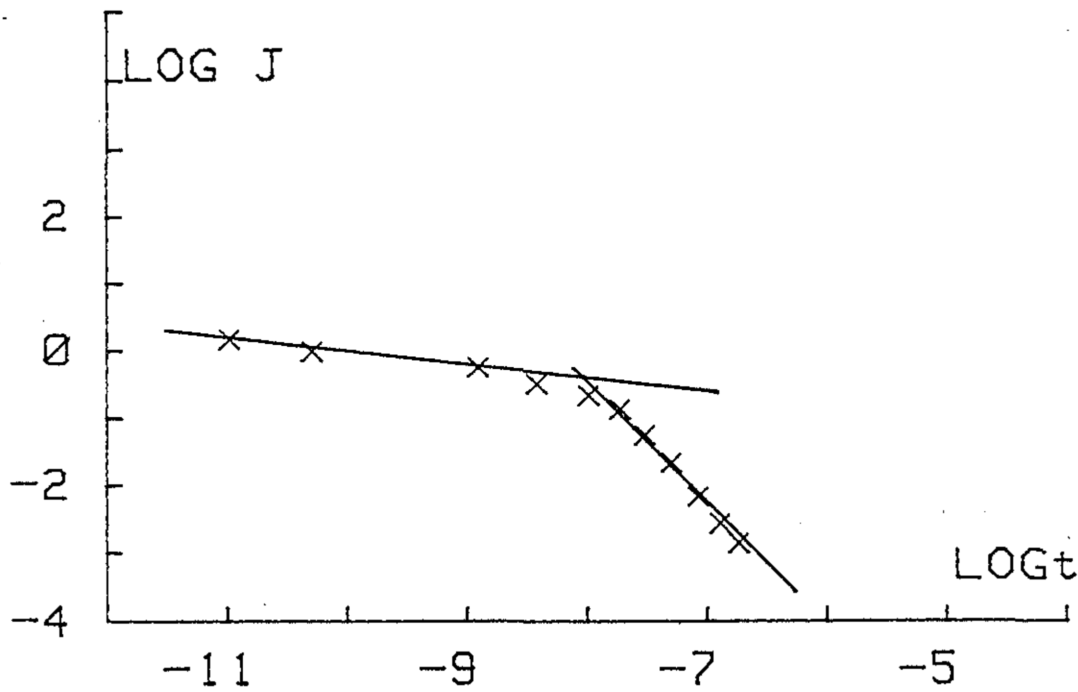

Fig 3.5: Logarithmic plot of transient photo-current in Se. (Observed at room temperature

3.3 Multiple-Trapping Model

The other mechanism which may bring about dispersive current behavior is multiple trapping. Through the analysis of the role of trapping states of different distribution profiles, expressions describing transient photo-current in the ideal circuit of Fig.5.6 will be developed here.

The Poisson's equation and the charge continuity equation under a condition of no sources or sinks are vital for constructing master equations describing this flow process. These are

$$J_c(x,t) = e_o \, \mu_o \, n_c(x,t)F(x) \tag{3.30}$$

$$\frac{\partial J_c(x)}{\partial x} = - e_o \frac{\partial n(x,t)}{\partial t} \tag{3.31}$$

$$n(x,t) = n_c(x,t) + \int_0^\infty n_t(x,t,E)dE \tag{3.32}$$

Where n (x,t,E) is the density of trapped electrons at x at the moment t in the energy range E and E + dE and other parameters have their usual meaning. The time independent applied field F(x) is considered to be almost uniform through the sample. Hence, taking the divergence of Eq.3.30 and equating with 3.31 gives

$$\mu_o F \frac{\partial n_c}{\partial x}(x,t) + \frac{\partial}{\partial t} n(x,t) = 0 \tag{3.33}$$

The kinetics governing the rate change of trapped electrons in the process of release from trapping sites followed by a subsequent retrapping

events can be put as[8,28]

$$\frac{\partial}{\partial t} n_t(x,t,E) = \frac{g(E)}{\tau_o N_t} n_c(x,t) - \frac{N_c}{\tau_o N_t} e^{-E/KT}_{nt(x.t.E)} \tag{3.34}$$

τ_o is the average life time of carriers in the conduction state. Here, energy is measured from the lower edge of the conduction band and we shall omit the superscript indicating energy reference (Chapter I).

Initial and boundary conditions used to solve the above set of equations consist the following: Prior to photogeneration, the material is considered to be in thermal equilibrium with a constant conduction current density under the influence of the applied field F. i.e.,

$$J_{co} = e_o \mu_o n_{co} F = cons \tag{3.35}$$

For a uniform generation of carriers following the photo-excitation, the density of carriers just after illumination is

$$n(x,o) = n_{ot} + n_{co} \doteq n_o \tag{3.36}$$

(Since concentration of photo-injected carrier $\gg n_o$ in insulating materials). Because nearly no electron found in traps at the instant just after illumination,

$$n_t(x,o,E) = 0 \tag{3.37}$$

In later times following the photo-generation, the sheet of charge drifts toward the collecting electrode at $x = L$ under the action of external electric field. This results a current. There is also trapping

and releasing events by localized trapping states. At equilibrium, carrier transfer rate equibalances and no net change in trapped and free carrier concentration happen. It is the contrary which is true for non equilibrium behavior. The contribution of freed carriers from traps decrease as their energy go further deep (Eq.3.34). Hence, if E^* is an energy such that the probability for releasing carriers from traps approach unity at a later time t then the probability for a release event to occur for $E > E^*$ is unlikely in this moment. i.e.,

$$\frac{N_c}{\tau_o N_t} t \; e^{-E^*(t)/KT} = 1 \tag{3.38}$$

Thus, for $0 < E < E^*$ equilibrium behavior exhibited

for $E > E^*$ non-equilibrium behavior exhibited

This leads to

$$\frac{\partial}{\partial t} n_t(x,t,E) = 0 \quad \text{for} \quad 0 < E < E^*(t) \tag{3.39}$$

Combining Eqs.3.34, 3.38 and 3.39 one will obtain

$$n_t(x,t,E) = \frac{g(E)}{N_c} e^{E/KT} n_c(x,t) \qquad E < E^*(t) \tag{3.40}$$

and

$$\frac{\partial}{\partial t} n_t\,(x,t,E) = \frac{g(E)}{\tau_o N_t} n_c\,(x,t) \qquad E > E^*(t) \tag{3.41}$$

From Eq.3.38

$$E^*(t) = KT \,\ln\left(\frac{N_c}{N_t} \frac{t}{\tau_o}\right) \tag{3.42}$$

Then Eq.3.41 solved to give

$$n_t(x,t,E) = \frac{g(E)}{\tau_o N_t} \int_o^t n_c(x,t')dt' \qquad \text{for} \quad E > E^*(t) \tag{3.43}$$

With this Eq.3.32 rewritten as

$$n(x,t) = n_c(x,t) + \int_0^{E^*(t)} n_t(x,t,E)dE + \int_{E^*(t)}^{\infty} n_t(x,t,E)dE \qquad (3.44)$$

Substituting for n (x,t,E) from Eqs.3.40 and 3.43 yields

$$n(x,t) = n_c(x,t) + \frac{n_c(x,t)}{\theta(t)} + \frac{1}{\tau(t)} \int_0^t n_c(x,t')dt' \qquad (3.45)$$

Where
$$\frac{1}{\theta(t)} = \int_0^{E^*(t)} \frac{g(E)}{N_c} e^{E/KT} dE \qquad (3.46)$$

and
$$\frac{1}{\tau(t)} = \frac{1}{\tau_0} \int_{E^*(t)}^{\infty} \frac{g(E)}{N_t} dE \qquad (3.47)$$

When $E > E^*(t)$ Eq.3.45 reduces to

$$n(x,t) \simeq n_c(x,t) + \frac{1}{\tau(t)} \int_0^t n_c(x,t)dt' \qquad (3.48)$$

For a strong non equilibrium condition, i.e., when the majority of carriers get immobilized by traps situated in deeper levels

$$n(x,t) \approx \frac{1}{\tau(t)} \int_0^t n_c(x,t')dt' \qquad (3.49)$$

The applicability criterion of this approximation can be put interms of mathematical expression as

$$\frac{1}{\theta(t)} n_c(x,t) \ll \frac{1}{\tau(t)} \int_0^t n_c(x,t')dt' \qquad (3.50)$$

After differentiating both sides of Eq.3.49 with respect to x and comparing the result with Eqs.3.33 and 3.36 we will get

$$\mu_o F \tau(t) \frac{dn}{dx}(x,t) = -(n(x,t)-n_o) \qquad (3.51)$$

Solving for n(x,t) gives

$$n(x,t) = n\,[1-e^{-\frac{x}{\mu_o F \tau(t)}}] \qquad (3.52)$$

When Eq.3.31 solved for conduction current density at x = L, one obtains

$$J_c(L) = -\; e_o \frac{\partial}{\partial t} \int_o^L n(x,t)dx \qquad (3.53)$$

The measured current J(t), under this experimental condition is simply the space average conduction current,

$$J(t) = \frac{1}{L} \int_o^L J_c(x,t)dx \qquad (3.54)$$

In light of Eq.3.53, this can be written interms of total carrier concentration as

$$J(t) = -\frac{e}{L} \frac{\partial}{\partial t} \int_o^L n(x,t)(L-x)dx \qquad (3.55)$$

This is the measurable current in the idealized external circuit of Fig.5.6 following a short photo excitation process. It describes the time evolution of a packet of charge carrier in the sample.

Substituting Eq.3.52 in 3.55 and solving by use boundary conditions results

$$J(t) = \frac{e_o}{L} n_o \frac{\partial}{\partial t} \{ \mu_o FL \tau(t) - (\mu_o F \tau(t))^2 (1 - e^{-\frac{L}{\mu_o F \tau(t)}}) \} \tag{3.56}$$

For a strong non equilibrium situation $\frac{1}{\tau(t)}$ is very large. i.e., $\tau(t)$ is very small. Thus,

$$J(t) \approx e_o \mu_o n_o F \frac{\partial \tau}{\partial t} \qquad \text{for } t < t_r \tag{3.57}$$

For the counter situation, the exponential term in Eq.3.56 can be put interms of Taylor series expansion. Therefore, after substituting the swеries expansion, if simplified and higher orders of $1/\tau(t)$ neglected, the resulting asymptotic equation for J(t) will be

$$J(t) \approx -\frac{e_o L^2 n_o}{\alpha \mu_o F} \frac{d}{t}(1/\tau(t)) \qquad \text{for } t > t_r \tag{3.58}$$

This branch of the asymptotic J(t) characteristic equation describes the rapid current drop behavior. The time corresponding to the transition from slower (3.57) to more rapid (3.58) current drop is defined to be the transit time t_r.

Through the application of the general relations derived above we shall examine the situation for typical trap distributions in the following sub-sections. Some materials show dispersive photo conductive property in transient photoconductivity experiments and witness the existence of single trap energy by other experimental techniques (such as TSC). In addition, a single energy level with sharp demarcation lacks the probability spread of trapping kinetics. Thus, the consideration of monoenergetic traps is evidently out of the issue as it is also very unlikey to find localized

trapping states in amorphous semiconductors with such feature. Our discussion then accounts for exponential and Gaussian distributions.

a) Gaussian Distribution

If the energy distribution profile of traps is considered to have a Gaussian nature:

$$g(E) = \frac{N}{\sigma\sqrt{\pi}} \; e^{-\left(\frac{E-E_t}{\sigma^2}\right)^2} \qquad (3.59)$$

Then, Eq.3.47 yields

$$\frac{1}{\tau(t)} = \frac{1}{\sigma\,\tau_o\sqrt{\pi}} \int_{E(t)}^{\infty} e^{-\left(\frac{E-E_t}{\sigma^2}\right)^2} dE \qquad (3.60)$$

Where erfc(x) = 1-erf(x) and $\mathrm{erf}(x) = \frac{2}{\sqrt{\pi}} \int_{0} e^{-\xi^2} d\xi$ (3.61)

Therefore,

$$\tau(t) = 2\tau_o\left[\mathrm{erfc}\left(\frac{E^*(t)-E}{\sigma}\right)\right]^{-1} \qquad (3.62)$$

Differentiating Eq.3.62 with respect to time results

$$\frac{d\tau(t)}{dt} = \frac{4\tau_o}{\sigma\sqrt{\pi}} \; e^{-\left(\frac{E^*-E_t}{\sigma^2}\right)^2} \left[\mathrm{erfc}\left(\frac{E^*-E_t}{\sigma}\right)\right]^2 \frac{dE^*(t)}{dt}$$

But from Eq.3.42

$$\frac{dE^*(t)}{dt} = \frac{KT}{t} \qquad (3.63)$$

Hence,

$$\frac{d\tau(t)}{dt} = \frac{4\tau_o KT}{\sigma\sqrt{\pi}\; t} \; e^{-\left(\frac{E^*-E_t}{\sigma^2}\right)^2} \left[\mathrm{erfc}\left(\frac{E^*-E_t}{\sigma}\right)\right]^{-2} \qquad (3.64)$$

Substituting for $\frac{d\ (t)}{dt}$ in Eq.3.57 yields

$$J(t) = \frac{4\, e_o n_o \mu_o F \tau_o}{\sigma\sqrt{\pi}} \; \frac{KT}{t} \; e^{-\left(\frac{E^*-E_t}{\sigma^2}\right)^2} \left[\mathrm{erfc}\left(\frac{E^*-E_t}{\sigma}\right)\right]^{-2}_{t<tr}$$

Similarly, differentiating Eq.3.60 by t provides

$$\frac{d}{dt}\left(\frac{1}{\tau(t)}\right) = -\frac{1}{\sqrt{\pi}\,\tau_o\, t}\ \frac{KT}{\sigma}\ e^{-\frac{(E^*-E_t)^2}{\sigma^2}}$$

Substituting this in Eq.3.58 results

$$J(t) = \frac{e_o n_o L^2}{6\sqrt{\pi}\,\mu_o F\tau_o}\ \frac{KT}{\sigma}\ \frac{1}{t}\ e^{-\frac{(E^*-E_t)^2}{\sigma^2}} \qquad t > t_r$$

The above asymptotic Eqs.(3.65 and 3.67) can further be simplified for the situation $\frac{E^*(t)-E_t}{\sigma} > 1$ by employing the following approximation relations[8.29].

$$\text{erf}x \simeq 1 - \frac{e^{-x^2}}{\sqrt{\pi}\,x}$$

$$\frac{E^*(t)-E_t}{\sigma} \simeq \frac{E^*(t)}{\sigma} \qquad (3.68)$$

By virtue of Eqs.3.38 and 3.68, Eqs.3.65 and 3.67 will then be rewritten as

$$J(t) = 4\sqrt{\pi}\ e_o n_o \mu_o F\ \frac{KT}{\sigma}\ \frac{N_c}{N_t}\ e^{E_t^2/\sigma^2}\ \left(\frac{E^*(t)}{\sigma}\right)^2 \left(\frac{N_c}{N_t}\frac{t}{\tau_o}\right)^{\beta-1} \qquad t < t_r \qquad (3.69a)$$

$$J(t) = \frac{e_o}{6\sqrt{\pi}}\ \frac{n_o L^2}{\mu_o F}\ \frac{KT}{\sigma}\ \frac{1}{\tau_o^2}\ \frac{N_c}{N_t}\ E^{-E_t^2/\sigma^2}\ \left(\frac{N_c}{N_t}\ \frac{t}{\tau_o}\right)^{-\beta-1} \qquad t > t_r \qquad (3.69b)$$

Where

$$\beta = \left(\frac{E^*(t)-2E_t}{\sigma^2}\right) KT \qquad (3.70)$$

b) Exponential Distribution

For a double exponential distribution of the form

$$g(E) = \frac{N_t}{2S} \; e^{-\frac{(E-E_t)}{s}} \qquad (3.71)$$

Eq.3.47 will give

$$\frac{1}{\tau(t)} = \frac{1}{2S\tau_o} \int_{E^*(t)}^{\infty} e^{-\frac{(E-E_t)}{s}} \, dE \qquad (3.72)$$

Evaluating this integral results

$$\frac{1}{\tau(t)} = \frac{1}{2\tau_o} \; e^{Et/s} \; e^{-\frac{E^*(t)}{s}} \qquad (3.73)$$

Using Eq.3.38 this becomes

$$\frac{1}{\tau(t)} = \frac{1}{2\tau_o} \; e^{Et/s} \; \left(\frac{N_c}{N_t}\frac{t}{\tau_o}\right)^{-\frac{KT}{s}} \qquad (3.74)$$

Therefore,

$$\frac{d\tau(t)}{dt} = 2KT \; \frac{N_c}{N_t} \left(\frac{N_c}{N_t} \; \frac{t}{\tau_o}\right)^{\frac{KT}{s}-1} \qquad (3.75)$$

and

$$\frac{d}{dt}\left(\frac{1}{\tau(t)}\right) = \frac{-KT}{2\tau_o^2 s} \; \frac{N_c}{N_t}\left(\frac{N_c}{N_t} \; \frac{t}{\tau_o}\right)^{\frac{-KT}{s}-1} \qquad (3.76)$$

Substituting for $\frac{d\tau(t)}{dt}$ and $\frac{d}{dt}\left(\frac{1}{\tau(t)}\right)$ in Eqs.3.57 and 3.58

$$J(t) = 2e_o\mu_o \; n_oF \; \frac{N_cKT}{N_tS} \; e^{-Et/S} \left(\frac{N_c}{N_t}\frac{t}{\tau_o}\right)^{-(1-KT/S)} \qquad t < t_r \qquad (3.77a)$$

$$J(t) = \frac{e_oL^2n_o}{12\mu_oF\tau_o^2} \; \frac{N_c}{N_t}\frac{KT}{S} \; e^{Et/S} \left(\frac{N_c}{N_t}\frac{t}{\tau_o}\right)^{-(1+KT/S)} \qquad t > t_r \qquad (3.77b)$$

It is worth to notice that Eqs.3.77 are obtained on the basis of $E^*(t) > E_t$. Otherwise Eq.3.72 will result $\psi(t) \approx 2\tau_o$ which can never explain dispersive transport. This indicates that majority of carriers are get immobilized in deeper trap levels.

The transient photo-current pulse predicted by Eqs.3.69 and 3.77 has a general feature

$$J(t) \sim t^{-(1-\alpha)} \qquad t < t_r$$

$$J(t) \sim t^{-(1+\alpha)} \qquad t > t_r$$

Which is identical with that suggested by hopping model Eqs.3.28 and 3.29.

Computer simulated logarithmic plots of the set of Eqs.3.69 and 3.77 are shown in Figs.3.6 and 3.7. Obviously, the transit time "t_r" can be infered from the intersection of the two branches of the log j - log t plot. On the other hand, if the transit time value of $E^*(t)$ is defined to be the activation energy, then by Eq.3.38

$$t_r = \tau_o \frac{N_t}{N_c} e^{Ea/KT} \qquad (3.78)$$

The slope $1/t_r$ Vs $1/T$ curve of Fig.3.8 provides the magnitude of this activation energy Ea. Since the drift mobility of charge carriers is inversely related to t_r, we can set

$$\mu \sim e^{-Ea/KT} \qquad (3.79)$$

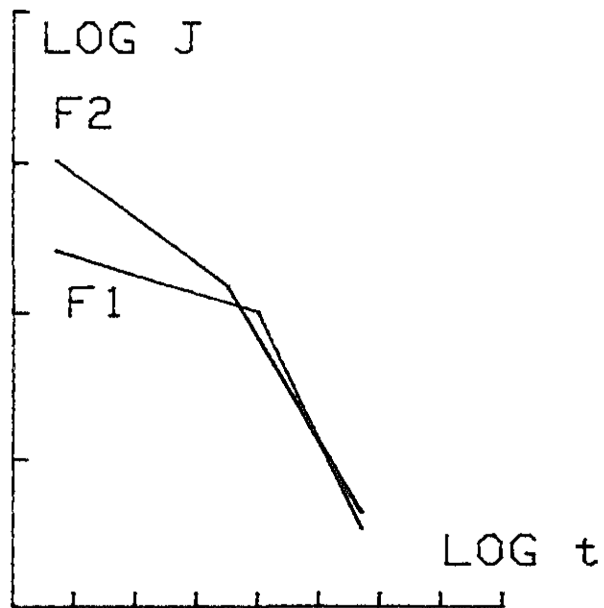

a) Gaussian distribution

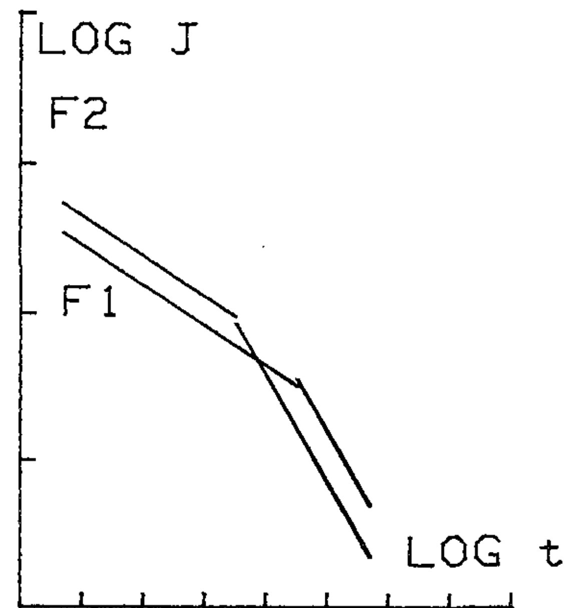

b) Exponential distribution

Fig.3.6: Simulated transient current pulse for different biasing fields. F2=10XF1

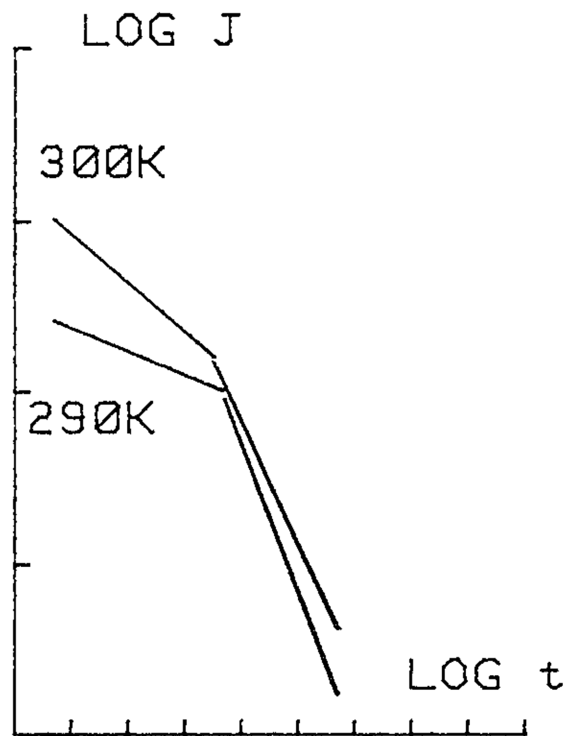

a)Gaussian distribution

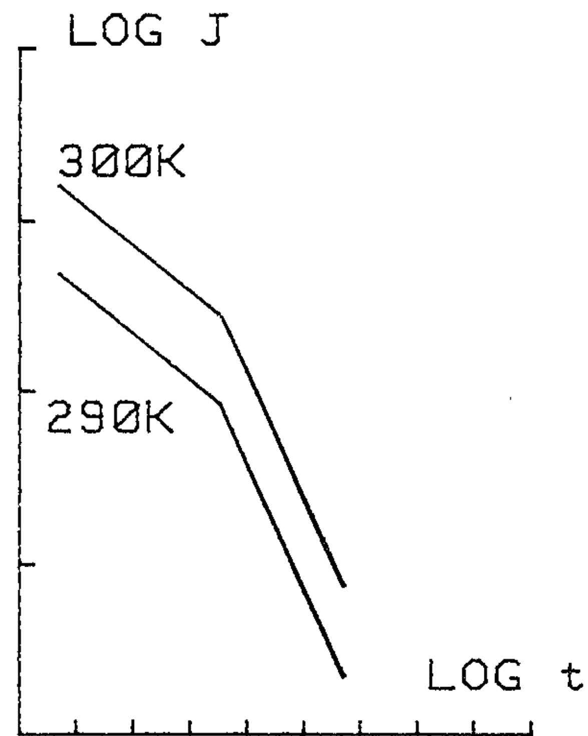

b)Exponential distribution

Fig.3.7:Simulated transient current pulse for different temperature. F=50000V/cm

This result practically indicate the activated nature of drift mobility in dispersive transport predicted by mutlipple trapping model. It also agrees with an empirical relation put forward by Gill[21,30]

$$\mu = \mu_o \; e^{-\frac{\Delta}{KT_{ef}}} \tag{3.80}$$

Where Δ is the activation energy and

$$\frac{1}{T_{ef}} = \frac{1}{T_o} - \frac{1}{T} \tag{3.81}$$

T_o is a temperature at which family of curves (with F as a parameter) in a log μ V_S 1/T plot intersect. This is shown in Fig.3.9. Infact, the activation energy is generally field dependent as several experimental results indicate. Thus, one can put

$$\Delta = \Delta_o - W(F)$$

Where Δ_o and $W(F)$ are the field independent and field dependent terms respectively.

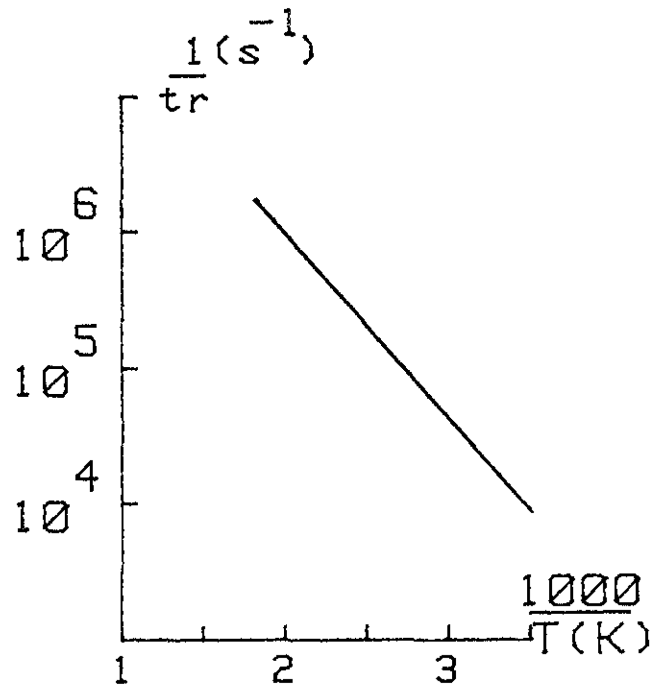

Fig 3.8: Activated nature of transit time.

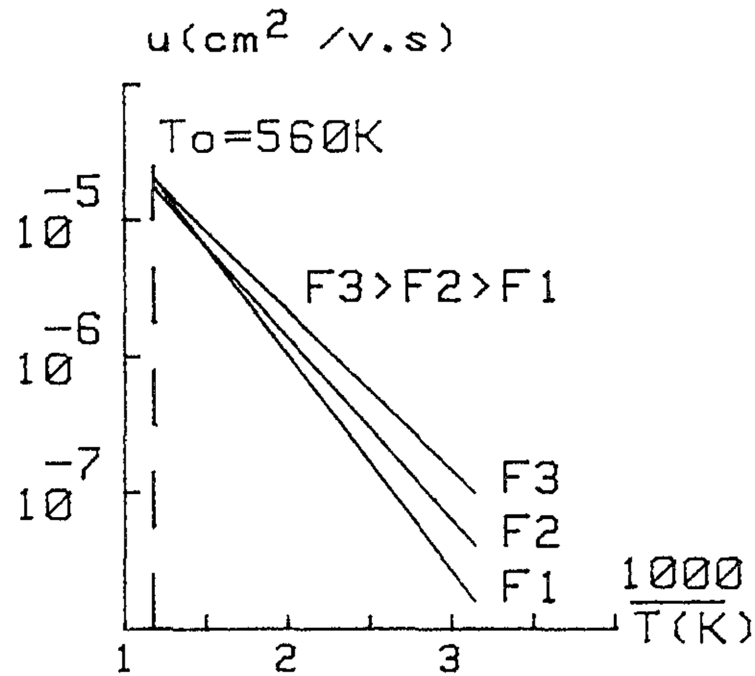

Fig 3.9: Drift mobility for different sweep field

($Nc=10^{21}$ (cm-3), $Nt=2\times10^{17}$ (cm-3), $to=10^{-8}$s)

CHAPTER IV

THERMALLY STIMULATED CURRENT IN AMORPHOUS SEMICONDUCTORS

The measurement of thermally stimulated current (TSC) have been used to determine parameters of traps in a wide calss of solids[31-33]. The main experimental technique consists photoexcitation of carriers by illuminating the sample (as in the preceeding chapter) accompanied by cooling to low temeprature so as to fill trapping centers. The sample then subjected to a heat source that can provide a uniform rate of temperature increase. Thermally stimulated current resulting from such a heating process in the dark then measured with temperature as a parameter. In this chapter a short theoretical review of thermally stimulated current is presented.

4.1 Classical TSC Equations

In describing TSC characteristics in solids having discreter energetic trap distributions, the kinetics to be solved may be described by the following set of equations[31]

$$\frac{dn_{ti}}{dt} = -\nu_i e^{-Et_i/KT} + \omega_i n_c Nt_i \tag{4.1}$$

$$\frac{dn_c}{dt} = -\sum_i \frac{dn_{ti}}{dt} - \frac{n_c}{\tau_c} \simeq 0 \tag{4.2}$$

Where ν_i , ω_i denote the frequency factor and capture coefficient of traps respectively. τ_c is effective life time of conduction carriers and all other parameters are as in former chapters. The index i indicates para-

meters to correspond to traps at level i. Energy measurement is from band edges.

From Eqs.4.1 and 4.2

$$\frac{dn_{tj}}{dt} = -(1-P_j)\nu_j e^{-Et_j/KT}_{nt_j} + P_j \sum_{i \neq j} \nu_i e^{Et_i/KT} \quad (4.3)$$

$$P_j = \frac{R_j}{1+\sum_i R_i} \quad \text{and} \quad R_j = \omega_j Nt_j \tau_c \quad (4.4)$$

Solving Eq.4.3 for monoenergetic trap distribution

$$n_t = n_t(0)\, e^{-\frac{\nu}{1+R} \frac{1}{\beta} \int_{T_o}^{T} e^{-Et/KT}} \quad (4.5)$$

With

$$T = T_o + \beta t \quad (4.6)$$

Where $n_t(o)$ is the initial occupancy of traps and β is the uniform rate of heating. Differentiating Eq.4.5 by t and combining the result with Eq.4.42 yields

$$n_c = \frac{\tau_c \nu}{1+R} e^{-E_t/KT} n_t(o)\, e^{-\frac{\nu}{1+R} \frac{1}{\beta} \int_{T_o}^{T} e^{-E_t/KT} dT} \quad (4.7)$$

Thus,

$$J(t) \sim \frac{\tau_c \nu}{1+R} n_t(o)\, e^{-E_t/KT}\, e^{-\frac{\nu}{1+R} \frac{1}{\beta} \int_{T_o}^{T} e^{-E_t/KT} dT} \quad (4.8)$$

Hence, the temeprature corresponding to the peak of TSC curve (satisfying $\frac{d\,J(t)}{dt} = o$ or $\frac{d}{dt} \ln J(t) = o$) is

$$\frac{1}{T_m} = \frac{K}{E_t} \ln \{ \frac{\nu K T_m^2}{(1+R) \beta E_t} \} \tag{4.9}$$

For two limiting cases,

negligible retrapping $(R \to o)$ $$\frac{1}{T_m} = \frac{K}{E_t} \ln \{ \frac{\nu K T_m^2}{\beta E_t} \} \tag{4.10}$$

large retrapping $(R \gg 1)$ $$\frac{1}{T_m} = \frac{K}{E_t} \ln \{ \frac{\nu K T_m^2}{R \beta E_t} \} \tag{4.11}$$

Thus, obviously R indicates the degree of retrapping unless have negligible effect. However, it is an over simplification to assume traps distribution with sharp demacration in the case of a-semiconductors. Most likely these materials rather posses continuous distribution profile of traps. To facilitate the discussion we consider the case of two sets of traps distributed in energy.

Assuming depper traps (E_2) involved actively as retapping sites and shallower traps dominantly releasing, Eq.4.3 gives

$$\frac{dn_{t1}}{dt} = - (1-P_1) \nu_1 e^{-E_{t1}/KT} n_{t1} \tag{4.12}$$

$$\frac{dn_{t2}}{dt} = P_2 \nu_1 e^{-E_{t1}/KT} n_{t1} \tag{4.13}$$

Solving Eq.4.12 for n_{t1}

$$n_{t1} = n_o e^{-\frac{(1+R_2)}{1+R_1+R_2} \frac{\nu_1}{\beta} \int_{T_o}^{T} e^{-E_{t1}/KT} dT} \tag{4.14}$$

From Eq.4.2

$$n_c \approx - \tau_c \left(\frac{dn_{t1}}{dt} + \frac{dn_{t2}}{dt}\right)$$

Hence, use of Eqs.4.12 and 4.13 results

$$n_c \approx \frac{\tau_c \nu_1 n_{ti}}{1+R_1+R_2} e^{-E_{t1}/KT} \qquad (4.15)$$

Substituting for n_{ti} from Eq.4.14 yields

$$n_c \approx \frac{n_o \tau_c \nu_1}{1+R_1+R_2} e^{-E_{t1}/KT} e^{-\frac{(1+R_2)}{1+R_1+R_2} \frac{\nu_1}{\beta} \int_{T_o}^{T} e^{-E_{t1}/KT} dT} \qquad (4.16)$$

Since $J(T) \cdot n_c$, the peak temperature therefore will be

$$\frac{1}{T_m} = \frac{K}{E_{t1}} \ln \left\{\frac{(1+R_2)\nu_1 K T_m^2}{(1+R_1+R_2)\beta E_{t1}}\right\} \qquad (4.17)$$

This roughly represents the low temperature peak of the resulting thermally stimulated current. If we completely neglect the effect of deeper traps level at the lower temperature TSC characteristics the results in Eqs.4.16 and 4.17 will be reduced to that of mono-energetic values. This shows that traps having large retrapping factor should influence the TSC spectrum by lowering peaks due to shallower levels. In fact carriers at deeper levels will be released in the temperature region of the second peak giving rise to an increase of its intensity.

From the above discussion one can see that the low temeprature peak of the two trap levels TSC spectrum is monitored by the parameters of the

deeper traps level (N_2). This information is consistent with Eq.4.4. Similar argument can then be employed for the situation of continuous distribution of traps in energy. This will be asserted as

$$R(E) = \omega \tau_c g(E) \tag{4.18}$$

where g(E) is the energy distribution of traps.

Thus, for continuous distribution of traps, carriers released from shallower traps during heating will get immobilized by deeper traps until major parts of carriers populated at a critical trap level which has greater retrapping factor R. A release from the critical trap level is therefore the dominant factor giving rise to the shift of TSC maximum towards higher temperature. However, for narrow distributions the TSC study can be reasonably approximated by expressions obtained for mono-energetic traps.

4.2 Field Dependent TSC

TSC characteristics observed in many a-semiconductors show electric field dependence[30,33-35] which is not describable by the classical approach (section 4.1). Hence, applicability question mark to the theory. A number of models have been developed[33-35] to give an explanation for the field dependent TSC.

If we introduce a temperature and field dependent rate of escape of carriers from traps[34]:

$$\nu(F,T) = \nu_o \, e^{-E/KT} R(F,T) \tag{4.19}$$

Where E is the depth of the trap, ν_o is the attempt-to-escape frequency (10^8-10^{13} Hz) and R(F,T) is the probability ratio which is equal to the ratio of escape rates in the presence and in the absnece of a field. The escape rate in the zero-field condition is

$$\nu(0,T) = \nu_o \, e^{-E/KT} \tag{4.20}$$

Then, for lower temperature peaks Eq.4.1 can be rewritten as

$$\beta \frac{dn_t}{dT} = -\nu(F,T) n_t(T) \tag{4.21}$$

Solving for n_t gives $n_t = n_{to} \, e^{-\{\frac{1}{\beta} \int_{T_o}^{T} \nu(F,T)dT\}}$ (4.22)

Thus, by Eq.4.2 $n_c(T) = \tau_c \nu(F,T) \, e^{-\{\frac{1}{\beta} \int_{T_o}^{T} \nu(F,T)dT\}}$ (4.23)

Therefore, $J_c(T) \sim \nu(F,T) \, e^{-\{\frac{1}{\beta} \int_{T_o}^{T} \nu(F,T)dT\}}$ (4.24)

The TSC peak temperature can be obtained from Eq.4.24 by the requirement $\frac{\partial J(T)}{\partial T} = 0$. This results

$$\left[\frac{\partial \nu(F,T)}{\partial T}\right]_{T=Tm} = \left[\frac{1}{\beta} \nu^2 (F,T)\right]_{T=Tm} \tag{4.25}$$

On the other hand, for temperatures not far from the initial temperature τ_o the exponential term in Eq.4.24 has a negligible contribution. Thus, we can write the formula describing the initial rise of the current as

$$J(T) = A\nu(F,T) \tag{4.26}$$

Where A is a constant. Let us now express the probability ratio by

$$R(F,T) = e^{\Delta/KT} \quad (4.27)$$

Where $\Delta \equiv \Delta(F)$ in general. Hence, from Eq.4.19

$$\nu(F,T) = \nu_o \, e^{-\left(\frac{\Delta_o - W(F)}{KT}\right)} \quad (4.28)$$

Substituting for ν (F,T) in Eq.4.26 we will get

$$T_m = \frac{1}{K} \frac{\Delta_o - W(F)}{\ln \left\{ \frac{\nu_o K T_m^2}{\beta(\Delta_o - W(F))} \right\}} \quad (4.29)$$

In the special case when the Poole-Frenkel behavior is observed

$$W(F) = \beta_{P,F} \, F^{\frac{1}{2}} \quad (4.30)$$

Where

$$\beta_{P,F} = \left(\frac{e_o^3}{\pi \varepsilon_o \varepsilon_r}\right)^{\frac{1}{2}} \quad (4.31)$$

Consequently the peak temperature (Eq.4.29) will be

$$T_m = \frac{1}{K} \frac{\Delta_o - \beta_{P,F} F^{\frac{1}{2}}}{\ln \left\{ \frac{\nu_o K T_m^2}{\beta(\Delta_o - \beta_{P,F} F^{\frac{1}{2}})} \right\}} \quad (4.32)$$

The initial rise of the current (Eq.4.26) can be computed using Eqs.4.26, 4.28 and 4.30. This yields

$$J(T) = \beta \, e^{-(\Delta_o - \beta_{P,F} F^{\frac{1}{2}}) KT} \quad (4.33)$$

The result in Eq.4.33 is identical with the expression proposed by

I. Chen[35] in his "mobility induced" TSC model set to describe TSC behaviors in hopping and multiple trapping systems.

While analysing observed TSC spectrum in systems showing field dependence behavior, we can put Eqs.4.29 and 4.33 as

$$T_m = \frac{1}{K} \frac{\Delta}{\ln\{\frac{\nu_o K T_m^2}{\beta\Delta}\}} \tag{4.34}$$

$$J(T) = \beta\, e^{-\Delta/KT} \tag{4.35}$$

The energy parameter "Δ" which may be field dependent in general can be put as

$$\Delta = \Delta_o + \gamma F^{\theta} \tag{4.36}$$

Where γ, θ are constants to be determined and Δ_o is the activation at zero field condition (they are least square fitted). Figs.4.1 and 4.2 illustrate calculated and experimentally observed field dependence TSC peak temperatures for PVK and mixtures of PVK-PC (polycarbonate)[34].

4.3 TSC Around the Glass Transition Temperature (Tg)

Study of thermally stimulated current in a number of polymers shows the existence of other TSC peaks associated to two relaxtion modes[32]:

i) TSC peak isolated around glass transition temperature T_g corresponds to a distribution of relaxation times following an Arrhenius equation.

ii) TSC peak observed at temperatures well above T_g is associated with the dielectric manifestation of liquid-liquid transition.

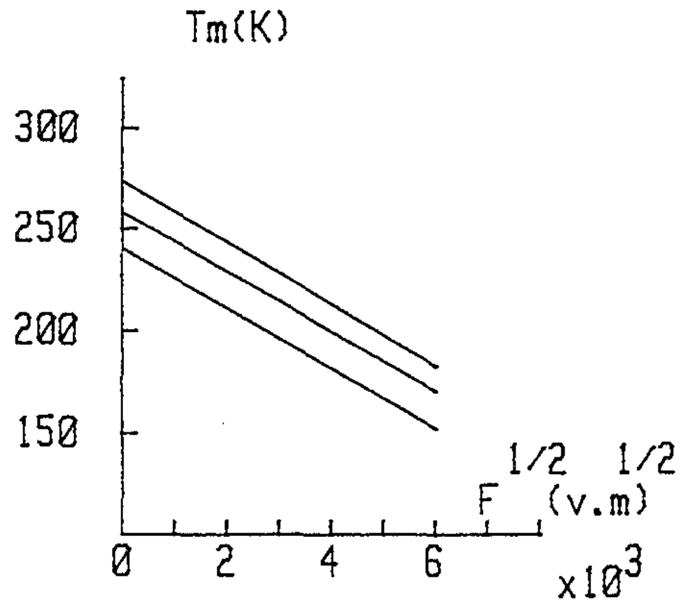

Fig 4.1: Field dependence of Tm calculated for Parameters £r=3,uo=10^{13}/s

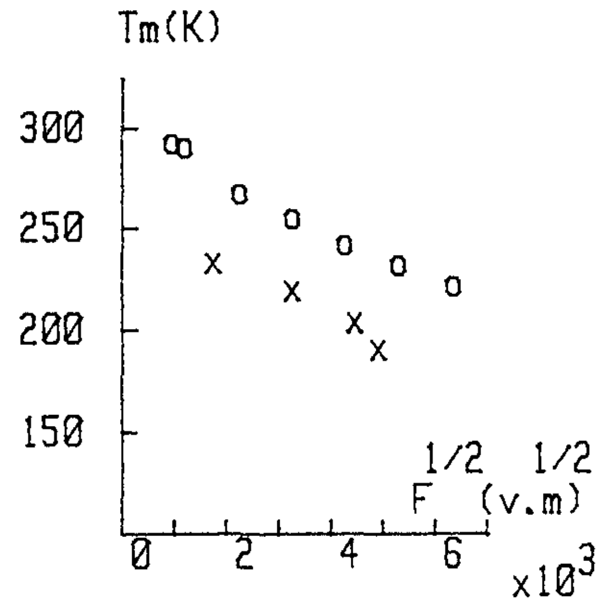

Fig 4.2: Observed field dependence of Tm for PVK(x) and mixture of PVK-60%W PC(o)

In the present discussion we concentrate on TSC peak of the first type.

For investigating the transition spectra of amorphous polymers, the following steps are used:

The sample will be polarized by an electric field F. When the polarization reaches its equilibrium value (P), the temperature will be lowered to freeze in this configuration. Then, the field will be cut off. The polarization recovery is then induced by increasing the temperature in a controlled manner. The measurement of this short circuit TSC therefore will allows us to deduce the relaxation time[36]

$$\tau = P/\sigma F \tag{4.37}$$

In the glass transition region the relaxation time often obeys the WLF empirical equation[37]

$$\tau(T) = \tau_o \, e^{-\frac{\tau_1 (T-T_g)}{\tau_2 + T - T_g}} \qquad T > T_g \tag{4.38}$$

Where C_1 and C_2 are constants. This can be converted into simpler Arrhenius formula. From Eq.4.38

$$\tau(T) = e^{-\frac{C_1 T}{C_2+T-T_g}} \; e^{\frac{C_1 T_g}{C_2+T-T_g}}$$

Introducing a relation $$T_\infty = T_g - C_2 \tag{4.39}$$

we will get $$\tau(T) = \tau_o \, e^{-C_1} \; e^{\frac{\tau_1 C_2}{T-T_\infty}} \tag{4.40}$$

Putting $$C_1C_2 = \frac{E_W}{K} \quad (4.41)$$

$$\tau(T) = \tau_{oa} \; e^{\frac{E_W}{K(T-T_\infty)}} \quad T > T_\infty \quad (4.42)$$

Where τ_{oa} is the product of τ_o and the first exponential term in Eq.4.40. Combining Eqs.4.42 and 4.37 provides the characteristic equation for the initial rise currents of TSC around T_g.

$$J(T) \approx A \; e^{-\frac{E_W}{K(T-T_\infty)}} \quad T > T_\infty \quad (4.43)$$

and A is a constant. Hence,

$$\ln J(t) \approx \text{cons} - \frac{E_W}{K(T-T_\infty)} \quad T > T_\infty \quad (4.44)$$

The slope of the initial rise TSC is therefore will help to deduce the activation energy. From Eq.4.44, the slope of $\ln J(T)$ Vs 1/KT curve is found to be

$$E_a \approx \frac{E_W}{1-T_\infty/T} \quad T > T \quad (4.45)$$

This result demonstrates the increase of the activation energy "Ea" with a decreasing temperature as the temperature approaches to T_∞. This is in confirmity with the exhibited apparent activation energy maximum near the glass transition temperature T_g[37,38].

During experimental observations, we practically encounter more TSC spectra as in Fig.4.3. Those peaks lying well below T_g are associated to TSC spectra we mentioned in earlier sections. The peaks at temperature well above T_g behaved to be due to the dielectric manifestation of liquid-liquid transitions. The complication will be avoided by employing partial

heating technique to the short circuit TSC measurements. Therefore, from the initial slope of each partial heating curve, the activation energy can be calculated[36,38].

CHAPTER V

ELECTRICAL CONDUCTION EXPERIMENTS

Electrical conduction experiments provide important informations on electronic properties of solids. This notion is clarified in the proceeding chapters. The present chapter consists experimental details of SCLC,TSC and transient photoconductivity in 2,4,7 trinitro-nine-flourenone and selenium. Structural formulas of these solids are given in chapter I.

In our experimental studies, we used sandwiched type samples that were prepared by vacuum evaporation technique. For the sake of high purity, the specimen were evaporated (3-4 times) on quartz substrates in a vacuum of 10-3Pa. In forming the sandwiched configuration, the metal electrode-TNF (or Se) - metal electrode were evaporated in succession with a rate of evaporation 0.5-1 nm/s at a substrate temperature 20oc for TNF (and 55oc for se).

Thickness and capacitance measurements were conducted by using Linnic interferometer and multi-frequency LCR meter respectively. Our experimental samples are

classified as shown in table 5.1 on the basis of the types of electrodes and thickness of the thin films of semi-conducting materials.

Temperature measurements were conducted with the help of chromel-copper thermocouple. The temperature readings were taken interms of mvs from the PM 2517E multimeter connected across the two dissimilar metals. Conversion of the thermal emf reading into oc has been made using the thermocouple calibration graph. The datas required for constructing the calibration graph were obtained by using the following experimental steps: One of the chromel-copper other junction was dipped in ice water mixture. The other junction was placed in an oven (consisting of electrical heater) together with a thermometer. The heater was regulated so as to raise the temperature in the oven slowly up to about 100oC and then the heating was stopped. Reading of thermal emf (from the multimeter) and the temperature reading on the thermometer were taken as the same time. This scale reading was carried until the temperature in the oven declines to room temperature.

During the measurement of the temperature of the sample kept in the oven, the thermocouple (once calibrated) hot junction has been put in close proximity

to the sample while the cold junction dipped in ice-water mixture.

5.1. SCLC experiments

The arrangement for SCLC measurements is as shown in Fig. 5.1. The apparatuses used are the following: Regulated power supply, BBC multimeter, measuring amplifier, electrical heater (oven), chromel-copper thermocouple, PM2517E multimeter.

For the investigation of SCLC characteristics in TNF and Se, samples AI and BI were used. The procedures followed in our experiment are:

a) With the arrangement as in Fig. 5.1 a potential difference (P.D) was set using the D.C. source. The voltage varied in steps. The resulted current reading was taken from the multimeter display. Through out the experimental time the temperature of the sample was checked from the PM 2517 multimeter display. The procedure was repeated for different similarily prepared samples.

b) The sample was kept in an oven. Biasing voltage was set fixed at values that were selected in the space charge region. For such particular P.d, the sample temperature was maintained at different values by

Table 5.1. Sample classification

Sample	Configuration	Film thickness (um)
AI	SnO_2-TNF-Al	8
AII	Ag-TNF-Al	4
BI	SnO_2-Se-Te	10
BII	SnO_2-Se ZnS	3

Table 5.2. Asymptotic equations of the Gaussian distribution.

Formula	Characteristic relation
I	$\xi\mu \frac{Nc}{Nt} \frac{V^2}{L^3} e^{\frac{-1}{kT}(E_t + \frac{\sigma^2}{2kT})}$
II	$e_o\mu Nc(V/L)e^{(\frac{-Et}{KT}+2)} e^{\frac{-1}{KT}\sqrt{2\sigma} \; 1+(2kT)^2 \; \ln \frac{e_oL^2A}{\varepsilon V}}$
III	$e_o\mu NC \frac{V}{L}^{l+1} \frac{e^{-Et/KT}}{(V_{TFL}-V)^{\ell}}$

*Et is the trap depth in this context

Table 5.3. parameters used in simulating the SCLC

Parameters	A-TNF	A-se
NC (CM-3)	$(2\pm1.4)\times10^{21}$	$(7 \pm 1.4)\times10^{18}$
Nt (Cm-3)	$(1\pm1.2)\times10^{17}$	$(3\pm1.2)\times10^{16}$
Et(e.v)	0.29 ± 0.04	0.11 ± 0.04
σ(e.v)	0.11 ± 0.02	0.07x0.02

regulating the heater and the magnitude of the space charge limited current reading and the corresponding temperature were recorded.

Results

For the polarity of the biasing field in Fig. 5.3. the observed SCLC characteristics account for electron current in TNF and hole current in Se. The evidence for this is followed from the comparisons made on the I-V behaviors resulted under changes of polarity of the applied P.D. In fig. 5.2. the situation for both biasing conditions is demonstrated. The sign of the biasing field resulting the I-V curve lying in the first quadrant is as depicted in Fig. 5.3.

The room temperature SCLC (flow of electrons in TNF and holes in Se) characteristics observed in the experiments are illustrated in Fig. 5.4. The cross marks in this diagram denote the experimentally obtained datas. The heavy lines drawn at the back ground of the experimental data curves are the computer simulated I-V characteristics for values of parameters given in table 5.3. (computer programs used for this simulation are given in appendix D). As it is manifested in the graphs, non-

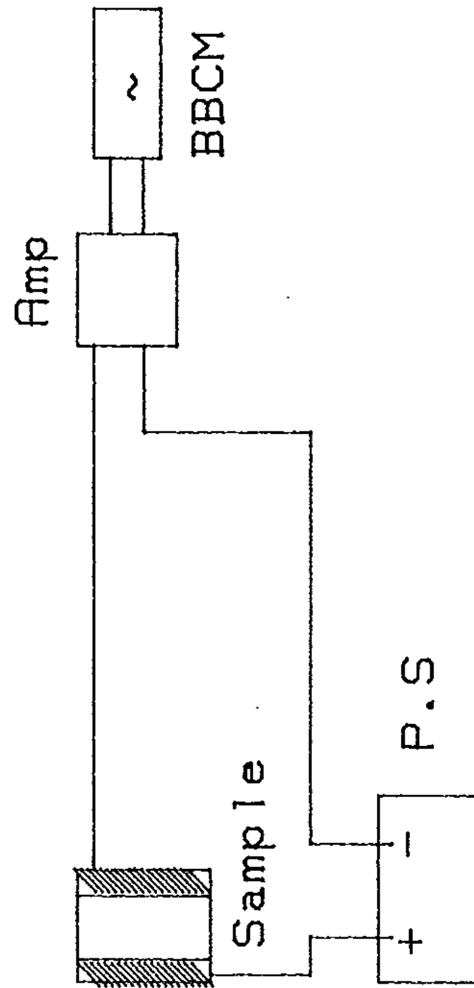

Fig 5.1:Circuit diagram for SCLC experiment.

linear I-V characteristics well observed at about 130-140 volts for TNF (sample AI) where as for Se (Sample BI) the non-linearity starts at about 4-6 volts. In both cases the steep portion of the experimental curve is well approximated by formula III for values of given in table 5.3. It is also clearly seen in the graphs that formula II nearly describe observed results well over a larger ranges of applied voltage.

Portions of the I-V characteristics that are approximated well by formula II exhibit a smoothly increasing behavior that can never be described by analytic equations we derived on the assumptions of mono-energetic and exponential distributions.

The other important behavior observed during an investigation of the temperature sensitivity of SCLC is demonstrated in Fig. 5.5. In contradiction to the characteristics predicted by mono-energetic and exponential distributions traps, the observed SCLC for both a-TNF and a-Se exhibits a non-linear dependence on the inverse of temperature. The computer simulated curves (heavy line) drawn by using formula II describe experimental results satisfactorily for the same values of parameters in table 5.3.

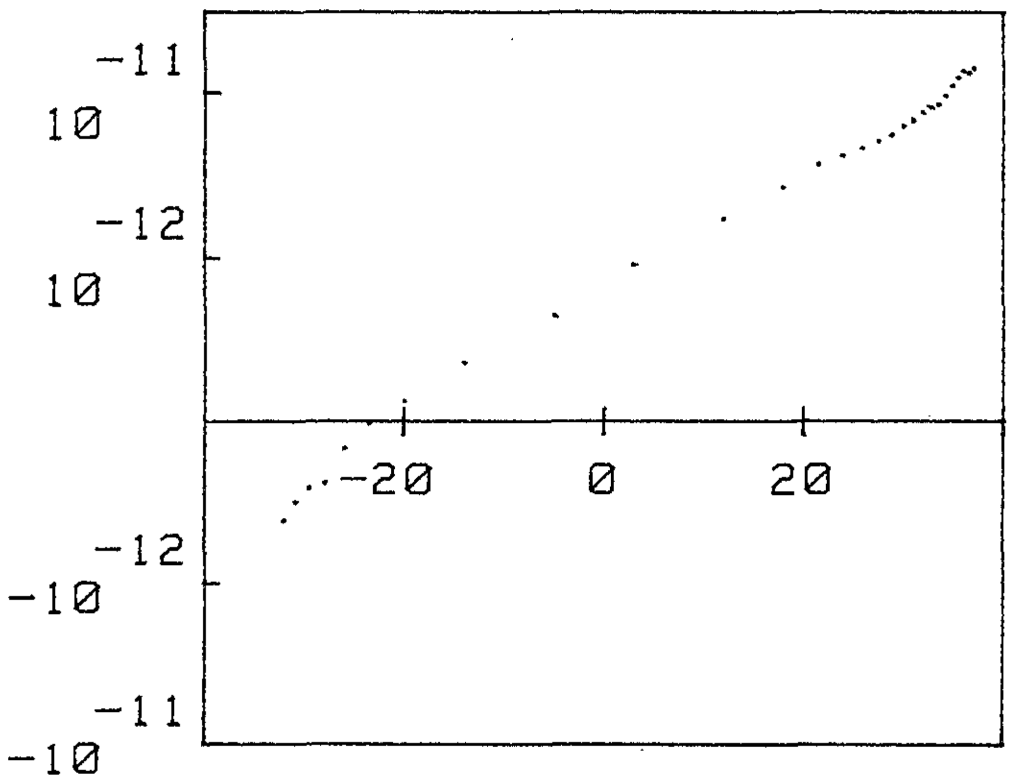

Fig 5.2a:SCLC(TNF) under change of polarity.

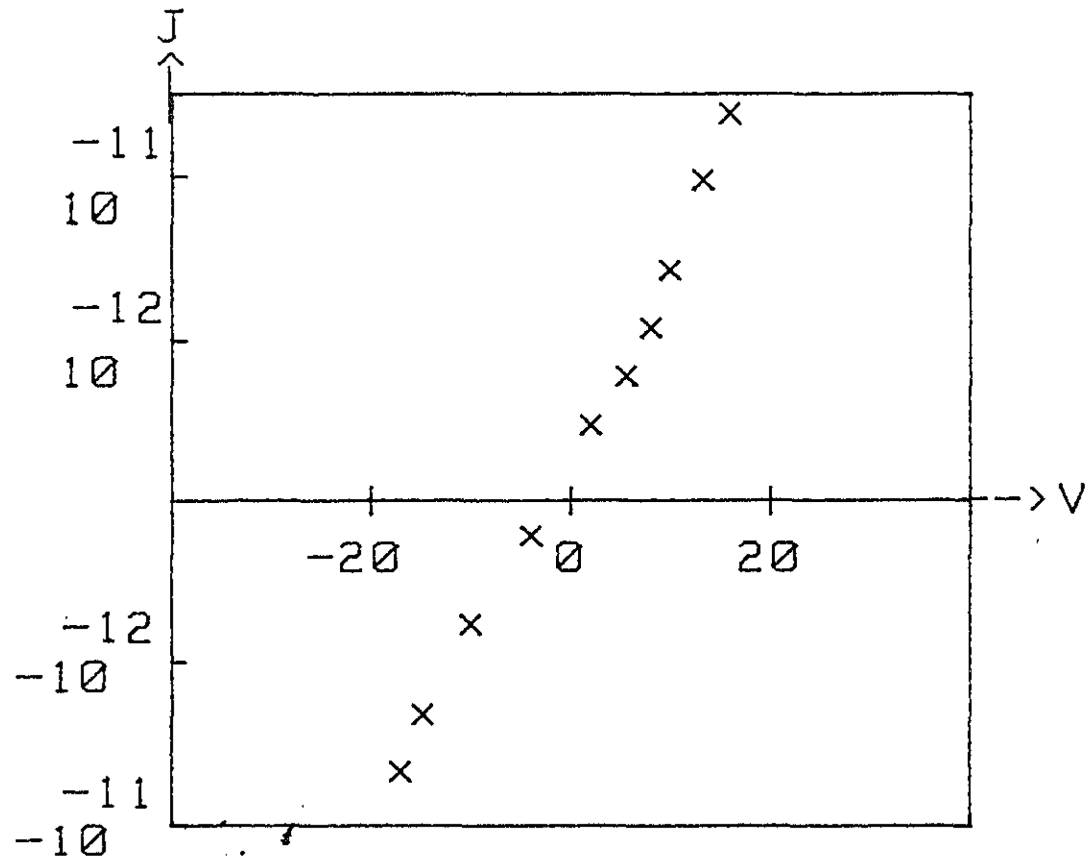

Fig 5.2b:SCLC(Se) under changes of polarity

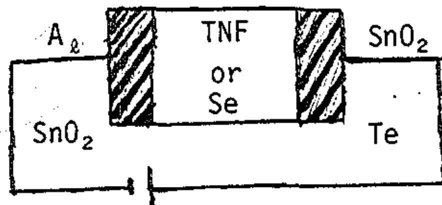

Fig.5.3 Polarity of the biasing field

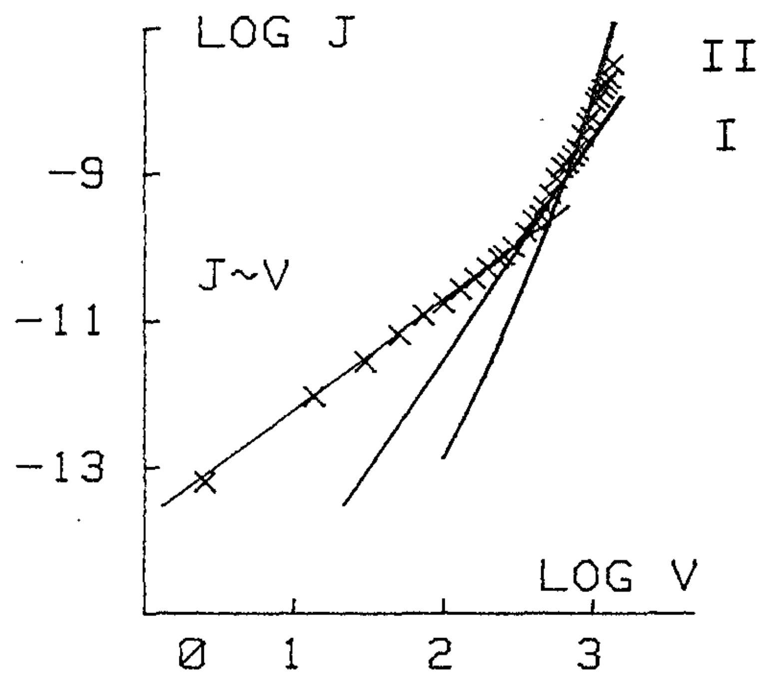

Fig 5.4a:SCLC in a-TNF(at room temperature)
Sample AI

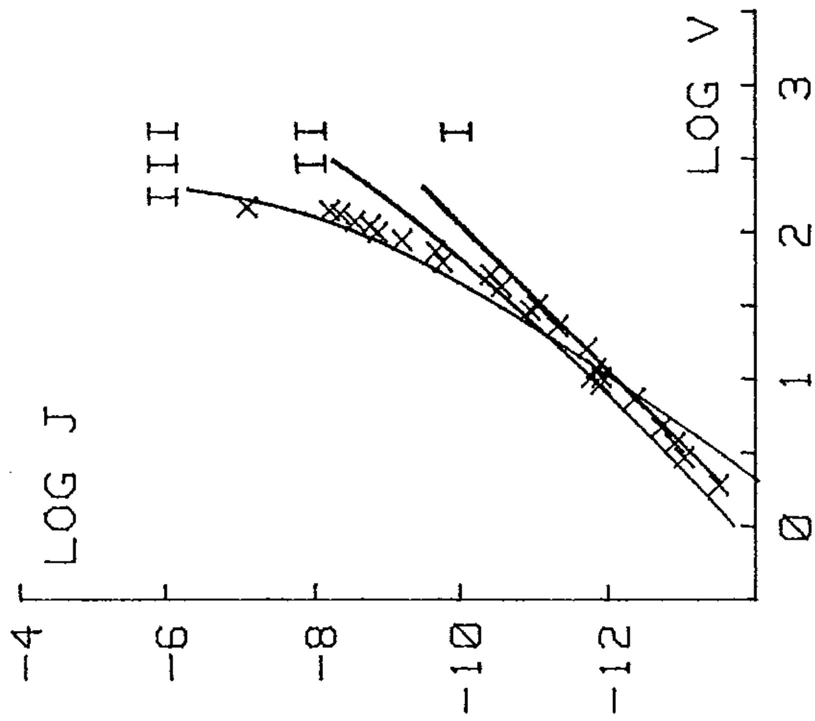

Fig 5.4b:SCLC in a-Se

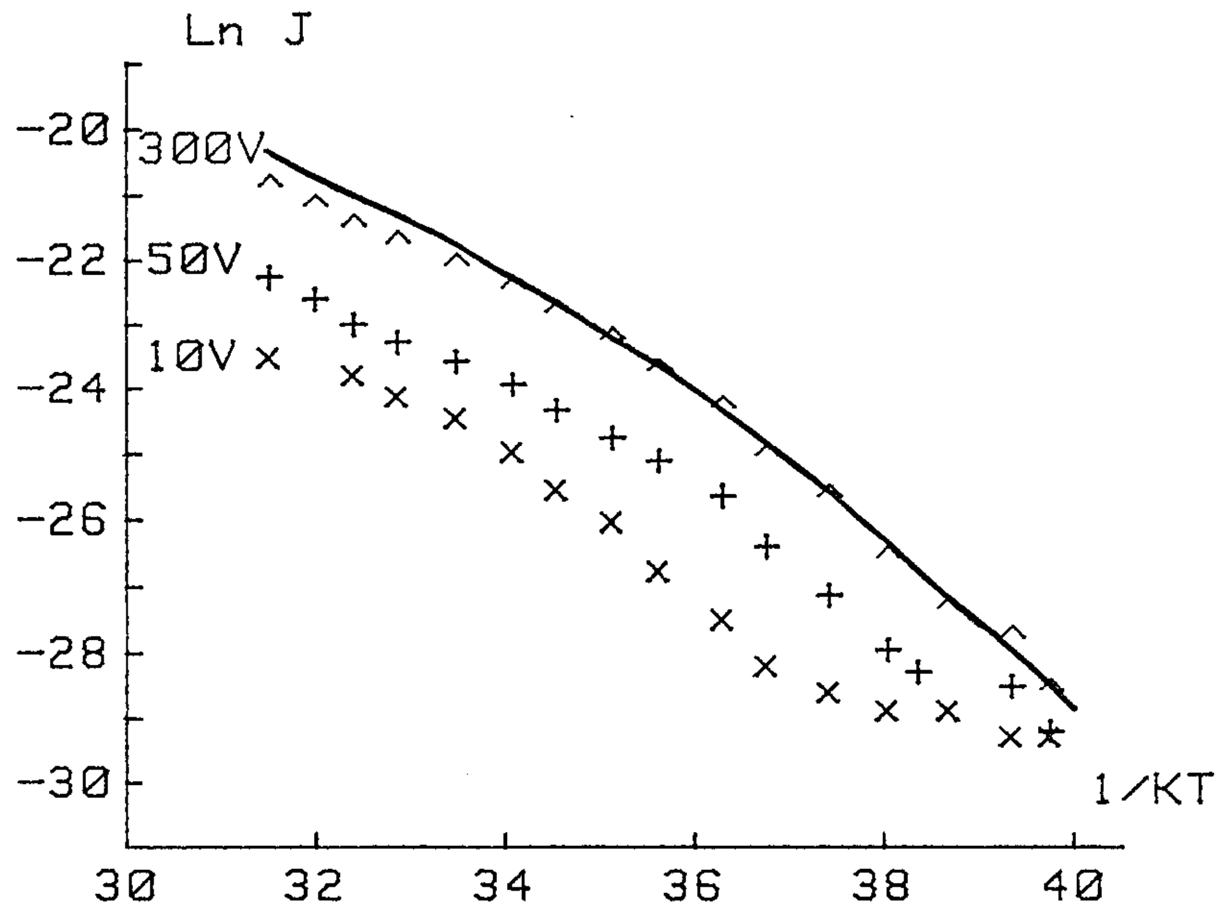

Fig 5.5a:SCLC dependence on T for a-TNF

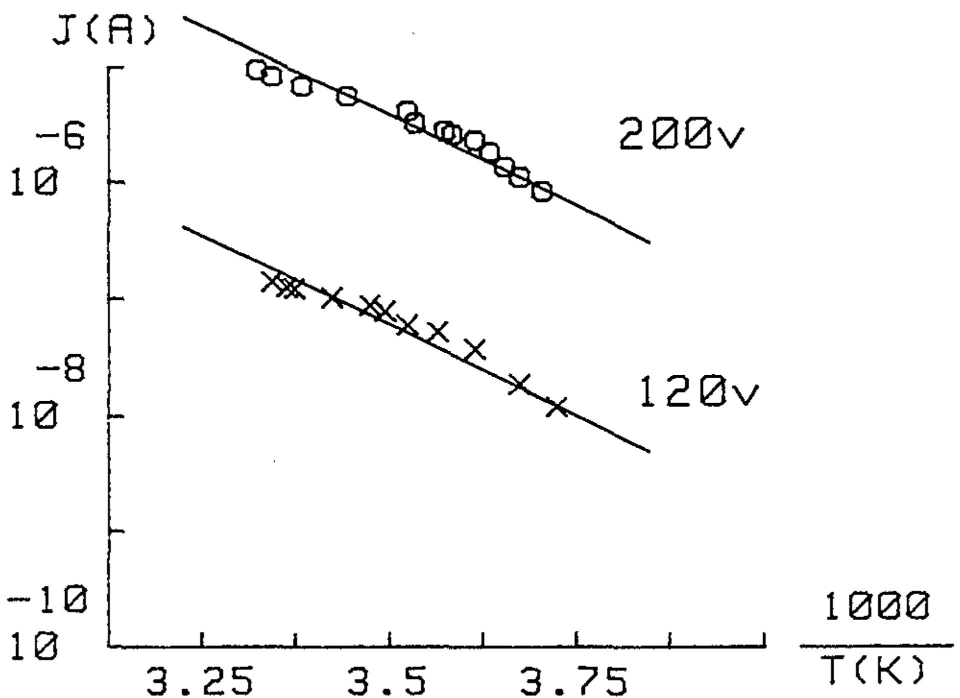

Fig 5.5b:SCLC dependence on T for a-Se

In summary, the observed SCLC behaviors that are illustrated in Fig. 5.4. and 5.5 witness infavour of the Gaussian distribution of traps with the best fitted values of parameters given in table 5.3. The computed values are reasonably close to results reported by other works [17,30]. We will further examine the extent these values agree with results obtained by other independent methods in the forthcoming sections.

5.2. Transient photoconductivity experiments

The experimental method employed involves the time-of-flight technique. The arrangement for this method is indicated in Fig. 5.6. Apparatuses we used in this experiment are: Xenon discharge lamp, regulated D.C. power supply, chromel-copper thermocouple, light filters, PM 2517E multimeter, 20MHZ Oscilloscope, regulated electrical heater (and heat insulating box), BBC multimeter, load resistor, 50cm focal length lens.

The choice of the load resistor was such that it avoids the effect of the measuring circuit response time on experimental results RC<<tr). The samples we used for this experiment were AII and BII types. The experimental procedures we followed were the following.

a. Samples were illuminated by pulsed light of 50 n.sec duration from the direction of Ag electrode for AII and NESA electrode for Se by xenon discharge lamp. The wave length of the photo-exciting light was 300n.m and 430n.m. for TNF and Se respectively. A P.d was applied instantly with the help of the D.C. power source. Datas of the resulted, current pulse

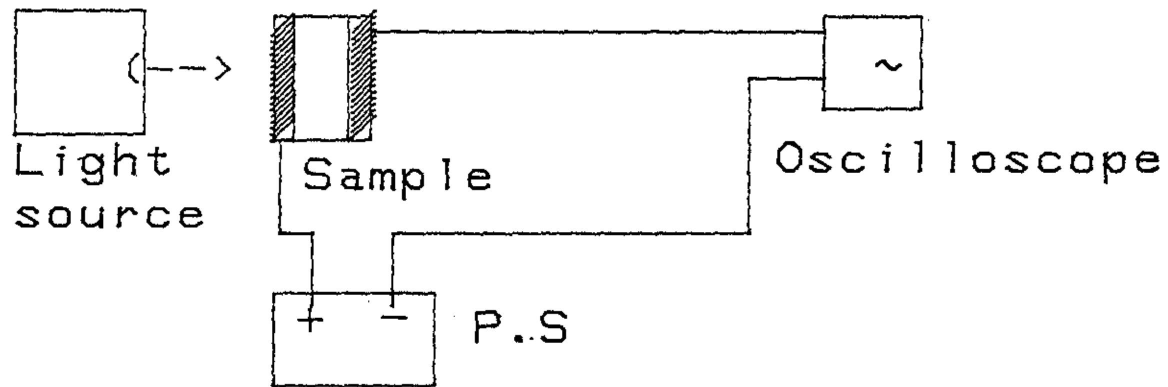

Fig 5.6: Circuit diagram for transient photoconductivity experiment.

was then taken from the oscilloscope display. For the same temperature, this step was repeated under different biasing voltage conditions.

b. Samples were kept in heat insulating box which itself placed 15cm above an electrical heater. The placement of the box was such that it particularly be under uniform heating. The heater was regulated (at a rate of 0.03k/5 on the average) inorder to maintain the temperature nearly at constant value during a single experimental run. For a fixed biasing voltage, measurements were conducted as in procedure "a", This step again repeated for different temperatures.

Note: To avoid unwanted excitations the samples were kept well away from infrared radiations.

Results

Typical transient current pulse shapes observed in our time of flight experiments are depicted in Fig. 5.7. These transient photocurrent pulse shapes were obtained by illuminating the samples from the direction of front

electrodes. The polarity of the drifting field was such that the front electrode is negative (or positive) with respect to the back electrode for sample AII (or sample BII). It is evident from the observation that holes in a-TNF and electrons in a-Se are get immobilized at their point of creations by the front electrodes. Therefore the observed transient current pulse shapes are accounted to electrons or holes flow in the bulk of a-TNF and a-Se respectively.

Fig. 5.8. illustrates the log I Log t characteristic curves of the transient current of Fig. 5.7. In this logarithmic plot, two branches are seen clearly. The two branches demonstrate the relatively slow (left) and rapid (right) current drops. This behavior is obviously consistent with the predictions of the theories (chapter 2). The set of transit time values determined for different experimental conditions from the intersections of the two branches are entered in table 5.4. Charge carriers drift mobilities again calculated from the obtained transit time values by using the conventional relation L/Ftr. The magnitudes of drift mobilities estimated in this manner are plotted in Fig 5.9. and 5.10.

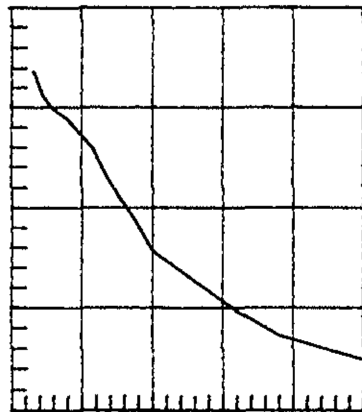

a)a-TNF.Sample AII

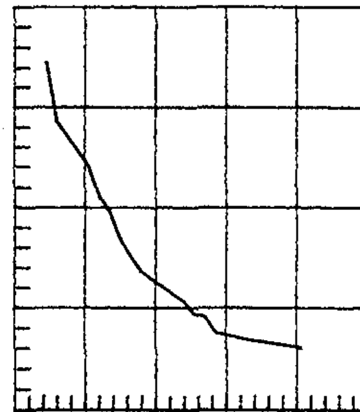

b)a-Se.Sample BII

Fig 5.7: Typical current pulse shape in a-TNF and a-Se at room temp.

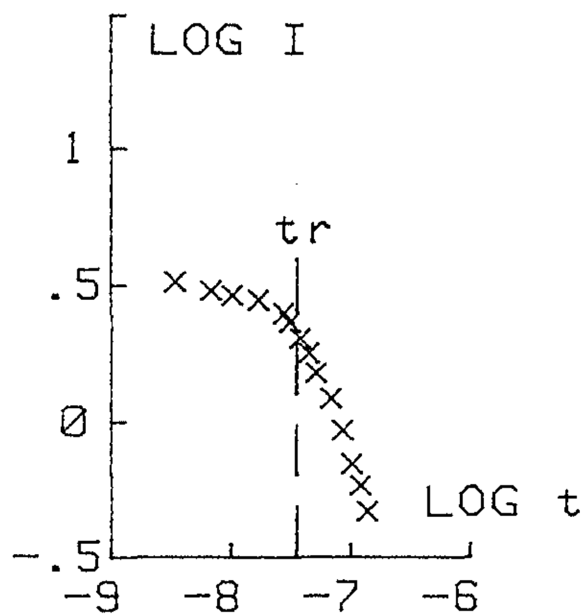

a)a-TNF

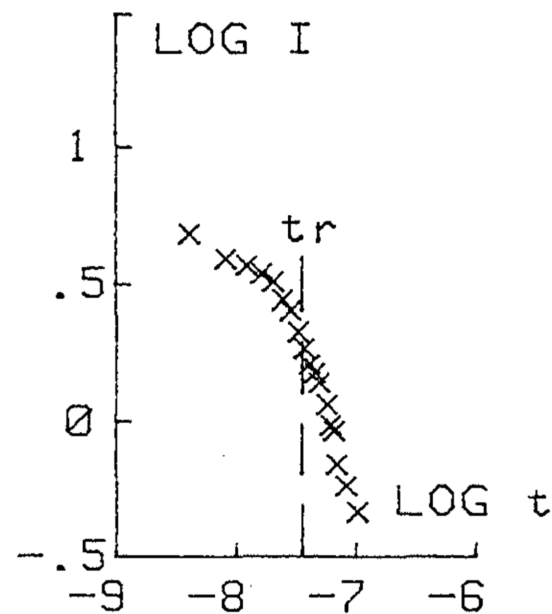

b)a-Se

Fig 5.8: Logarithmic plot of current pulse shape of Fig 5.7

Table 5.4

Transit time values computed from observed results

temperature Constant				field Constant			
TNF		Se		TNF		Se	
V(v)	t(m.s)	V(v)	t(ms)	T(K)	t(ms)	T(K)	t(ms)
16	6.7	5	1.46	290	2.26	290	.13
30	2.1	10	.38	294	2	292	.12
64	.5	15	.13	298	1.67	296	.11
90	.21	20	.065	305	.81	298	.10
120	.106	25	.034	310	.54	301	.097
		30	.018			303	.091
						305	.083

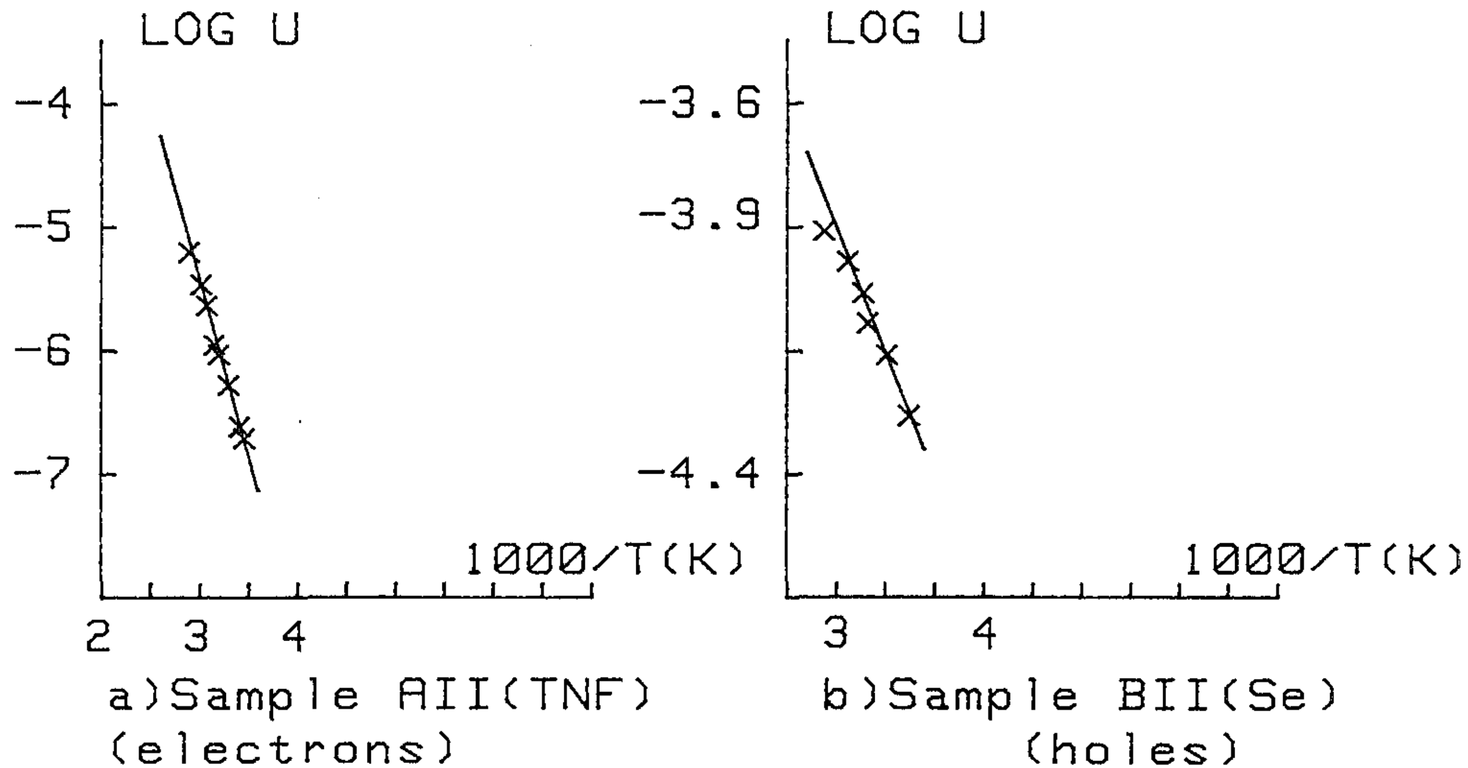

Fig 5.9: Temperature dependece of drift mobilities (at constant field)

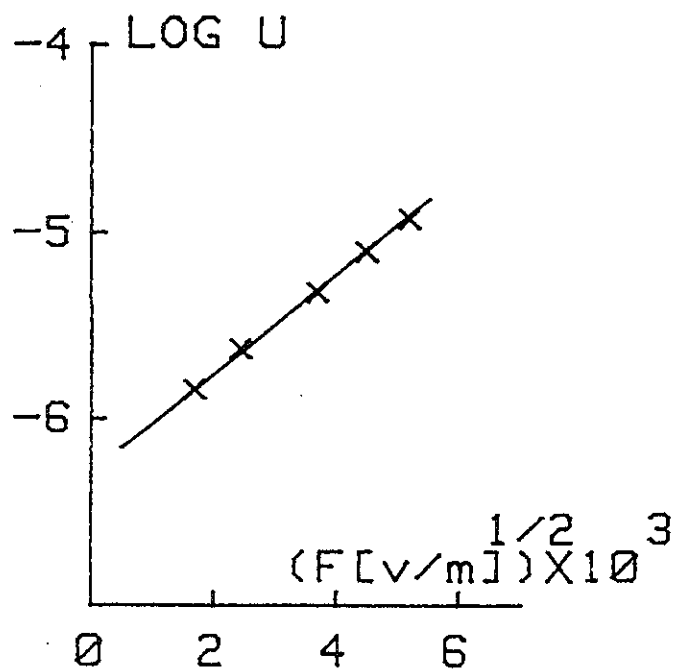

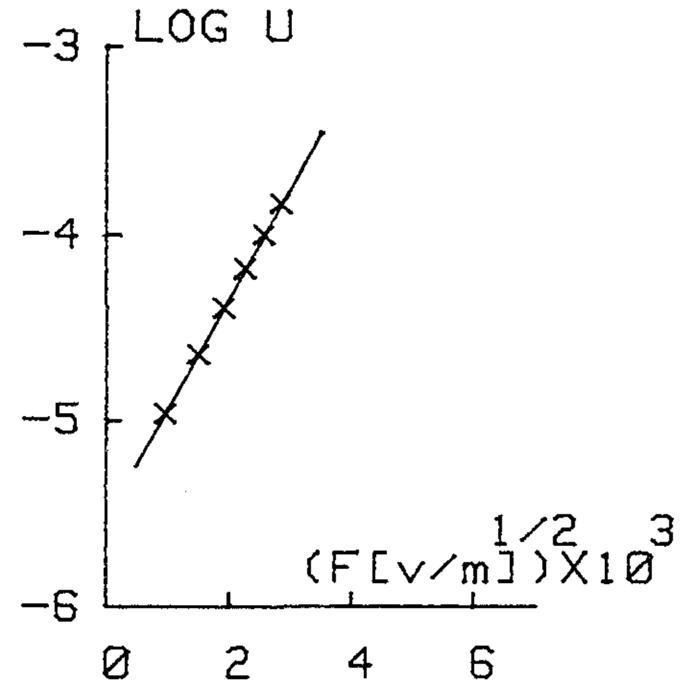

Fig 5.10: Field dependence of drift mobilty at room temperature

In Fig. 5.9. the change of drift mobilities with temperature is shown. The heavy lines drawn in contrast the experimentally computed values are representing the computer simulated results of eq. 3.80. In both a-TNF and a-Se, the observed temperature dependence of drift mobilities reveal the activated nature of charge carriers flow. This is evidenced by the well reasonable agreement between observation and simulated work in Fig. 5.9. This approximation of observed results provide values of activation energies $Ea=0.45\pm\ 0.03$ e.v for electron mobility in a-TNF at a field strength of $3x10^{5}$ v/cm and $Ea=0.24\ \pm0.02$ev for hole mobility in a-Se at a sweep field of value $3.3x10^{4}$v/cm. These values are practically agree with those reported by Gill and pfister from their respective work under the same experimental method [30,40]. Furthermore, these obtained values are found to be very close to energy parameters determined from the low temperature TSC peak [30]. In addition to this, the results of our experimental work suggest the magnitudes of electron drift mobilities in the order of 10-6cm /v.s. for electrons in a-TNF and 10-4 cm /vs for holes in a-Se.

In Fig. 5.10 electric field dependences of drift mobilities (at room temperature) are illustrated. As indicated in the diagram, drift mobilities in a-TNF and Se

exhibit a non linear variation with respect to a change in the sweep field. Rather drift mobility of electrons (in a-TNF) and holes (in a-Se) show a linear dependence on the square root of the applied field. The slopes of μ Vs F 1/2 curves of Fig. 5.10 are calculated to fit for the values $Bp.F = 2.6x10^{-4} e(Vcm)^{\frac{1}{2}}$ and $BP.F = 5.1 \; 10^{-4} e(V.cm)^{\frac{1}{2}}$ for a-TNF and Se respectively. When these parameters are evaluated by eq4.31 the result is εr=8.52 for TNF and εr=2.04 for Se. Since the obtained dielectric constants have the same order of magnitude as the corresponding values determined by other independent technique, the observed field dependence can be considered to be explainable interms of poole-Frenkel mechanism.

From results and the datas in Fig. 5.10 the zero field activation energies are also calculated. The activation energy of electrons in A-TNF is extrapolated to the zero field value of 0.61 $\pm$ 0.04 ev which is almost identical with the result by Hirisch,[30] The Zerofield extrapolated activation energy of holes in a-Se on the other hand is 0.41 $\pm$0.03 ev.

With regard to the popular believe; multiple trapping is the underlying mechanism for dispersive transport in a-Se, we shall next value the predictions of the multiple

trapping model from the standpoint of observed behaviors in a-Se. For the ranges of the applied fields and temperatures we have been working with, the fall of the transient current provides the values of in the range between 0.2 to 0.5. Since for the case of exponential distribution α =Kt/s, this suggests a dispersion parameter of the distribution "s" such that it is in the range 2-5. If dispersion parameter of such order is admitted in the analysis of SCLC, it will particularly leads to a result which is very contradictory to observations. The situation for the Gaussian distribution on the other hand is completely different. Surprisingly, the Gaussian distribution suggests a dispersion parameter in the order of 0.06 e.v. which is in agreement with the result in the SCLC analysis.

Further insight in the field dependence of transient current reveals the decrease of the parameter towards zero. This is directly manifested in the log I- Log t plot. As indicated in Fig. 5.11 the "Knee" of the logarithmic plot tends to disappear as the applied field increases. Obviously, this behavior can not be explained by exponential distribution profile in the temperature range of the experiment. The Gaussian distribution on the other hand can describe this characteristics if a field

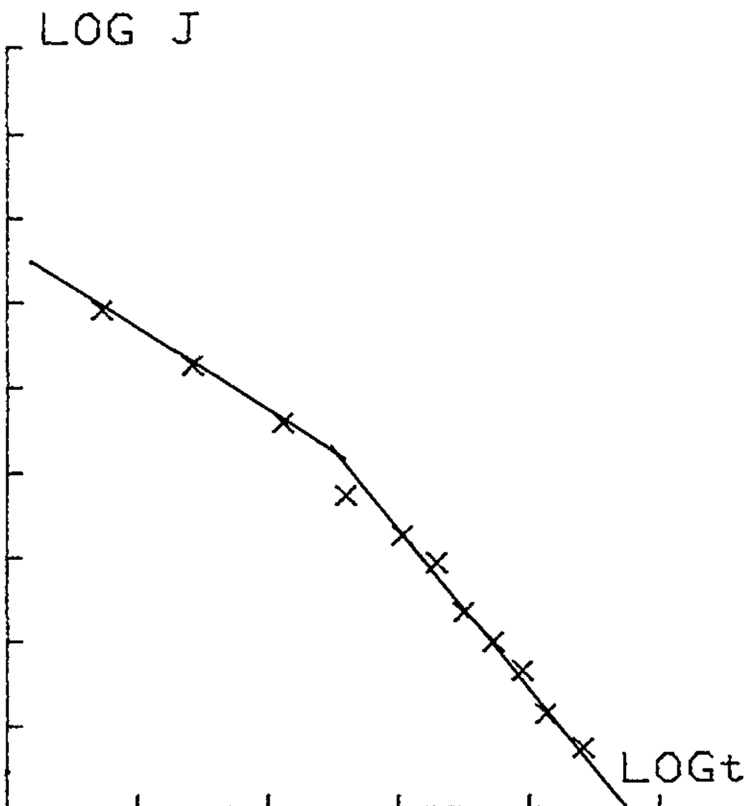

Fig 5.11: Transient current in Se for V=50v & T=291K

dependent activation energy is admitted in eq 3.70 (Fig. 3.7). Hence our preference of the Gaussian distribution in approximating the energy parameters (given above) from experimental curves.

In addition to the energetic parameters, the simulated I(t) behavior provides the following best fitted values for asymptomatic equations developed on the basis of Gaussian distribution: $NC = 6 \times 10^{19}$ $Nt = 2.2. \times 10^{15}$ $\tau_0 = 1.8x10-8$ 5 and $\sigma = 0.06ev$ The magnitude of the zero field activation energy and the trap depth estimated from our observations demand the dispersion parameter to be greater than 0.04ev. Values of σ less than 0.04 e.v. practically leads to the flattening of the left hand curve in the log-log plot of room temperature transient current. But this is very contrary to observations since it represents the approach towards ultimate equilibrium. The result therefore drives our intuition to the fact that the broadening of the dispersion of traps distribution hence the influence of traps situated at energies deeper than Et(from the band edge) will result the observed anomalous I(t) behavior. Infact it can be noted that the dispersion $\sigma = 0.06$ e.v is slightly higher than the energy frozen into the lattice (KTg) upon sample preparation. [2.4] Tg is order of 49o for selenium.

5.3. TSC experiments

Our experimental investigation was on the TSC characteristics near the glass transition temperature. The apparatuses involved in our measurements were D.C. power supply, chromel-copper thermo-couple, oven, y-t recorder.

Experimental study of TSC characteristics around Tg was conducted on AII type samples according to the following procedure: Sample was polarized under a polarizing field of $3x10^4$v/cm to $7.5x10^5$v/cm range for 10 minutes. The polarized sample then subjected to a uniform heating (0.1k/s on the average). To avoid infrared excitations, experiments were performed well in the dark. The magnitude of the thermally stimulated current was measured as a function of temperature. Current reading was aided by the recorder while the temperature measurement being as in the proceeding sections. The sensitivity and the speed of the recorder was selected at values 1mv/cm and 5mm/min respectively.

Results

In Fig. 5.12 the TSC spectrum of a-TNF around Tg is illustrated. This characteristics represent the

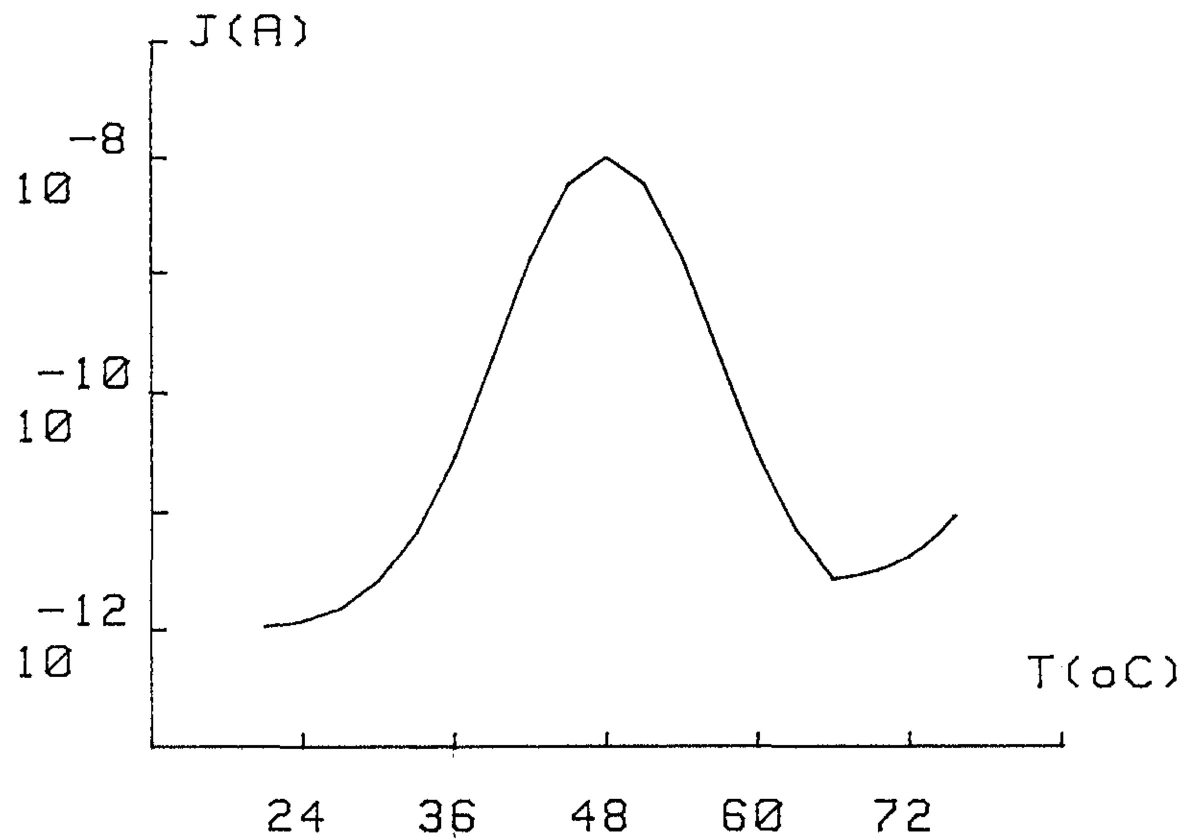

Fig 5.12:TSC spectra arround Tg for a-TNF

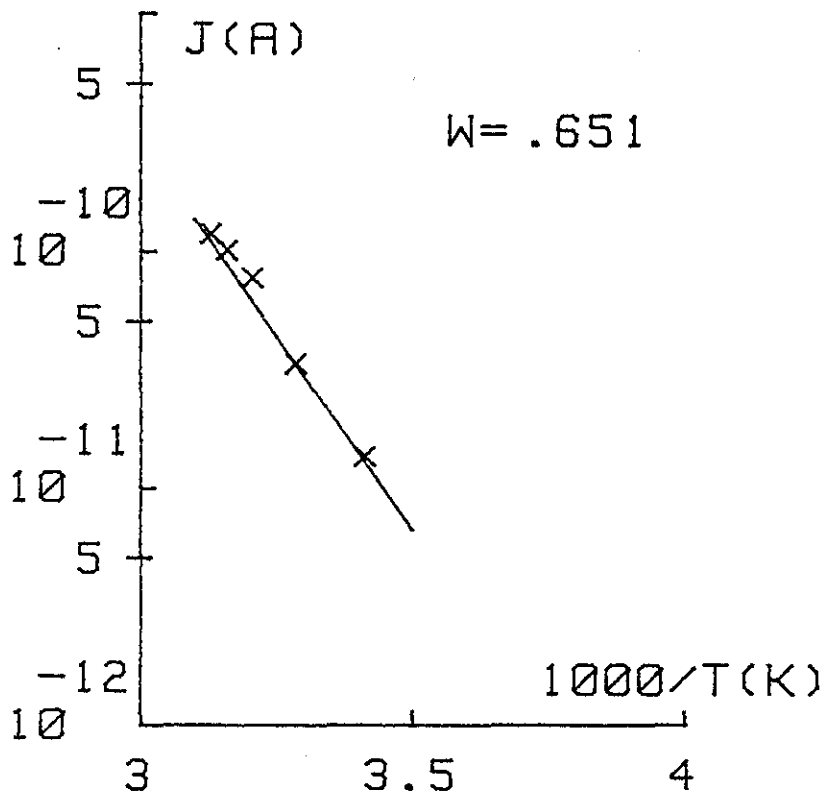

Fig 5.13: Experimental results of TSC observed in a-TNF

observations for a poling field of 7.5×10^5 v/cm. The initial rise portion of this experimental curve is depicted in the log I Vs $\frac{1}{T}$ graph of fig. 5.13. The slope of the later provides a value of 0.65 $\pm$ 0.02 e.v for the activation energy in a-TNF. Such an order of energy is very greater than the trap depth and true activation energies estimated in the proceeding sections. But, it has a striking similarity with the zero field extrapolated activation energy in a-TNF. This result therefore suggests that the activation energy determined from the initial rise portion of TSC around Tg is identical with the zero field extrapolated activation energy of drift mobility and thus containing the disorder-induced energy term. [24]

5.4 SUMMARY AND CONCLUSIONS

2,4,7 trinitro-nine-flourenone(TNF) and Selenium (Se) are semi conductors. (Where the former is an organic semiconductor. In their amorphous forms these semiconductors) possess a relatively large densities of states that can involve as charge carriers trapping centers. These localized states are very likely distributed in energy within the mobility gaps.

For estimating the parameters and distribution profiles of traps in a-TNF and a-Se, electrical conduction experiments can be used as a powerful means. The use of more independent types of conduction experiments practically will provide wide range of informations on the bulk electrical properties. Thus a much better approximated values of trap parameters are expected. The following few paragraphs present a summary of our results in a SCLC, TSC and transient photoconductivity experimental investigations made on a-TNF and Se.

SCLC, both in a-TNF and Se, exhibit a non-linear dependence on the applied voltage (Figs 5.4 and 5.5.). The observed I-V characteristics in these materials are found to be well describable by asymptotic equations developed in the basis of Gaussian distribution of traps. The physical indications of this is that it is very unlikely to assume traps to be concentrated at a single energy level with sharp boundaries. Rather they can be thought to show a smoothly varying distribution in energy. The assumption of a Gaussian distribution of traps (electron traps in a-TNF and hole traps in a-Se) describe the observed SCLC characteristics more satisfactorily with values of parameters indicated in Fig. 5.14 and table 5.5.

Table 5.5

Parameters determined from observed results

	Nc(cm-3)	Nt(cm-3)	Et(ev)	σ (ev)
TNF	$(2+1.4)\times10^{21}$	$(1+1.2)\times10^{17}$	.29+.04	.11+.02
Se	$(7+1.4)\times10^{18}$	$(3+1.2)\times10^{16}$	.11+.04	.07+.02

	Eao(ev)	$Bpf(e(v.cm)^{1/2})$	$u(cm^2/v.s)$
TNF	.61+.05	$(2.6+1)\times10^{-4}$	$\sim10^{-6}$
Se	.41+.02	$(5+1)\times10^{-4}$	$\sim10^{-4}$

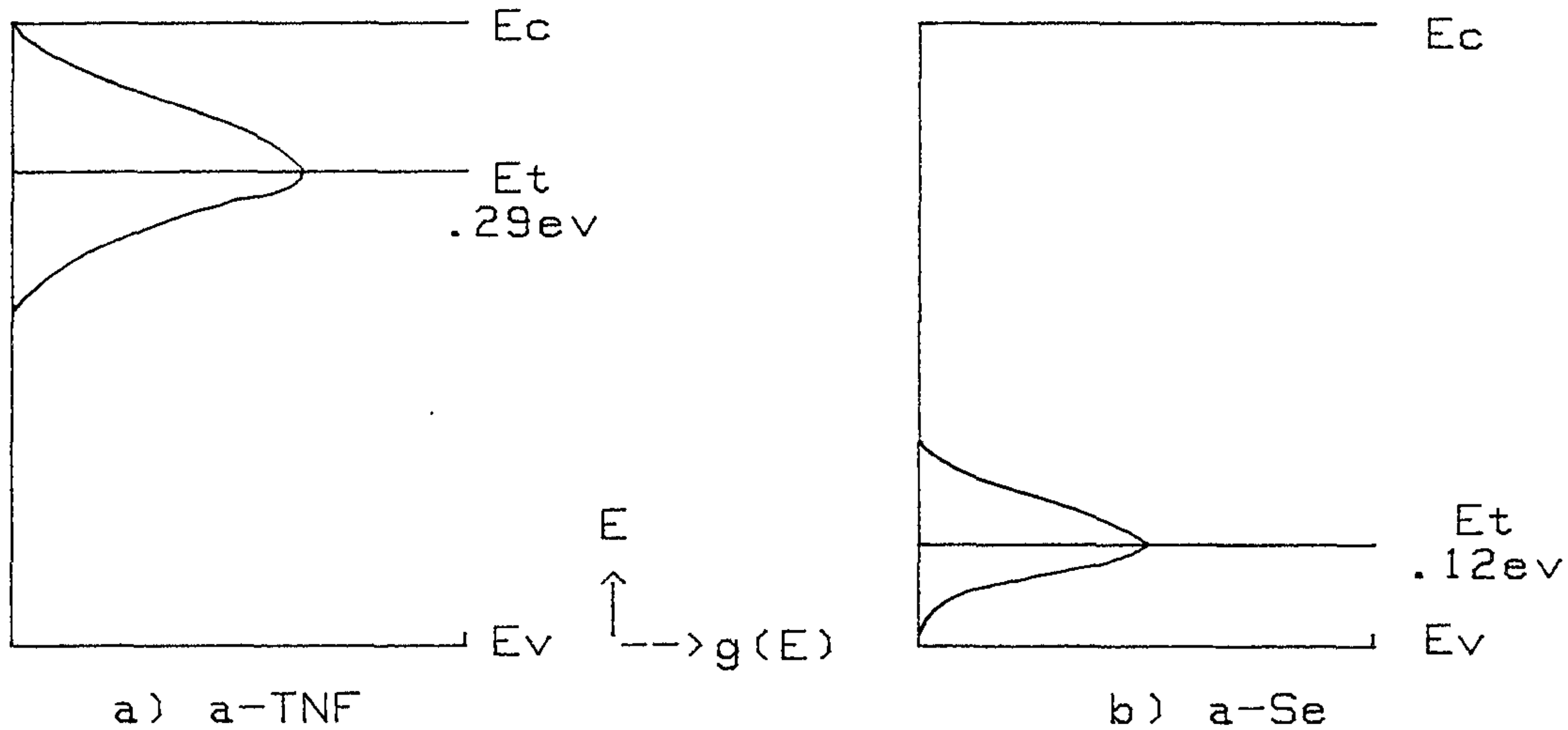

Fig 5.14: Energy distribution of traps
estimated from observation

The observed current pulse resulting from a short pulse photo-excitation of carriers shows a dispersive character. Electrons drift mobilities in a-TNF and holes mobilities in a-Se exhibit an activated behavior. The activation energies themselves are field dependent in a manner similar to that suggested by Poole-Frenkel mechanism. In regard to the inclination that multiple trapping is the responsible mechanism for a dispersive carrier flow in a-Se, the Gaussian model describe the experimental results very well with allowance of field dependent activation energy. Gaussian distribution of hole traps explain observed transient photoconductivity with the parameters given in table 5.5. These results are also found to agree quite reasonably with those obtained from SCLC study.

Our achievement from the TSC study near the glass transition temperature indicates the variation of the thermally stimulated current with temperature in an arrhenius manner. The activation energy for electron transport in a-TNF is 0.65 ev order as calculated from the initial rise portion of this TSC spectrum. This order of magnitude is remarkably very different from the activation energy estimated from the field dependent low temperature TSC peak (0.47 e.v) [30]. The obtained 0.65 e.v on the other hand shows a very close agreement with the zero

field extrapolated activation energy of electron mobility in a-TNF.

For the energy parameters (Et,Ea and Eao) deduced from our observations the coulomb trap model suggests a o.1ev (a-TNF) and a 0.07 e.v (a-Se) magnitudes of energy for the coloumb energy term [30]. These orders of energies are surprisingly equal to the dispersion parameters " σ " of our result.

APPENDIX A

TRAP OCCUPANCY ESTIMATION FOR LOW INJECTING LEVEL

From Eqs.2.7 and 2.8

$$\frac{\varepsilon}{e_o} k_1 k_2 V/L^2 = n_{cL} + n_{tL} \qquad \text{A1}$$

When trap filling process costs the dominant portion of injected carriers, Eq.A1 can be approximated as

$$\frac{\varepsilon}{e_o} k_1 k_2 V/L^2 \approx n_{tL} \qquad \text{A2}$$

a) If trap occupancy is given by

$$n_{tL} = \frac{N_t}{1+\frac{N_c}{N_{cL}} e^{-E_t'/KT}} ,$$

The second term in the denominator is very much larger than unity. Therefore, one can put

$$n_{tL} = n_{cL} \frac{N_t}{N_c} e^{-E_t'/KT} \qquad \text{A3}$$

Eq.A2 then will give

$$n_{cL} = \frac{\varepsilon}{e_o} k_1 k_2 \frac{V}{L^2} \frac{N_c}{N_t} e^{-E_t'/KT} \qquad \text{A4}$$

b) If trap occupancy is given by

$$n_{tL} = \frac{N_t}{2(s-1)} e^{-\frac{(E_t-E_L)}{S}} \quad e^{-\frac{(E_t-E_F}{KT}}$$

Combining this with Eq.A2

$$e^{E_F/KT} = \frac{\varepsilon}{e_o} k_1 k_2 \frac{V}{L^2} \frac{2(S-1)}{N_t} e^{\frac{(E_t-E_L)}{S}} e^{E_t/KT} \qquad \text{A5}$$

From Eq.2.4,

$$e^{E_F/KT} = \frac{n_{cL}}{N_c} e^{E_c/KT} \qquad \text{A5'}$$

Equating these two results

$$n_{cL} = \frac{\varepsilon}{e_o} k_1 k_2 \frac{V}{L^2} 2(S-1) \frac{N_c}{N_t} e^{\frac{(E_t-E_L)}{S}} e^{-E_t'/KT} \qquad \text{A6}$$

APPENDIX B

TRAP OCCUPANCY INTEGRAL EVALUATION

From Eq.

$$n_{tL} = \frac{N_t}{\sqrt{2\Pi}} \int_0^{Y_F} \frac{e^{-y^2/2}}{1+e^{\frac{1}{KT}(x-\sigma y)}} dy \qquad B1$$

$$Y = \frac{E_t - E}{\sigma} \; ; \quad Y_F = \frac{E_t - E_F}{\sqrt{2}\sigma} \; ; \; x = E_t - E_F$$

When injection level scans the lower tail of the distribution, with similar argument used in A2

$$n_{tL} = \frac{N_t}{\sqrt{2\Pi}} \int_0^{Y_F} e^{-y^2/2} \; e^{-\frac{1}{KT}(x-\sigma y)} \; dy \qquad B2$$

$$n_{tL} = \frac{N_t}{\sqrt{2\Pi}} \; e^{-x/KT} \, I \qquad B3$$

Putting
$$\xi = \frac{Y - \sigma/KT}{\sqrt{2}}$$

$$I = \sqrt{2} \; e^{\frac{\sigma^2}{2(KT)^2}} \int_{\xi_o}^{\xi_f} e^{-\xi^2} \, d\xi$$

Where $\xi_o = -\frac{\sigma}{KT\sqrt{2}}$ and $\xi_f = \frac{1}{\sigma\sqrt{2}} \{ E_t - E_F - \frac{\sigma^2}{KT} \}$

When $E_t - \frac{\sigma^2}{KT} > E_F$, for small dispersion parameter σ and temperature which is not very low $\xi_o \to 0$ and $\xi_f \to \infty$. Therefore,

$$I = \sqrt{2}\; e^{\frac{\sigma^2}{2(KT)^2}} \int_0^\infty e^{-\xi^2}\, d\xi$$

i.e.,

$$I = \frac{\sqrt{\pi}}{\sqrt{2}}\; e^{\frac{\sigma^2}{2(KT)^2}} \qquad \text{B4}$$

Substituting for I in B3 gives

$$n_{tL} = N_t\, e^{-\frac{1}{KT}\{E_t - E_F - \frac{\sigma^2}{2KT}\}} \qquad \text{B5}$$

Using Eq.A2 therefore results

$$n_{cL} = \frac{\varepsilon}{e_o} k_1 k_2 \frac{V}{L^2} \frac{2N_c}{N_t}\; e^{-E_t'/KT}\; e^{-\frac{\sigma^2}{2(KT)^2}}$$

or

$$n_{cL} \approx \frac{\varepsilon}{e_o} \frac{V}{L^2} \frac{N_c}{N_t}\; e^{-\frac{1}{KT}(E_t' + \frac{\sigma^2}{2KT})} \qquad \text{B6}$$

For the energy range $E_t - \frac{\sigma^2}{KT} < E_F < E_t$, it is rather impossible to evaluate the integral for trap occupancy directly from the equation. But we shall present mathematical steps leading to good approximation. Following the same argument we developed in the preceeding steps the trap occupancy for this superquadratic range can be put as

$$n_{tL} = \frac{N_t}{\sigma\sqrt{2\pi}} \int_{-\infty}^{\infty} \frac{e^{-\frac{(E-E_t)^2}{2\sigma^2}}}{1+e^{\frac{(E-E_F)}{KT}}} \qquad \text{B7}$$

Putting $Y = \frac{E-E_F}{KT}$ and $x = E_t - E_F$

$$n_{tL} = \frac{N_t KT}{\sigma\sqrt{8\pi}} \; e^{-x^2/2\sigma^2} \int_{-\infty}^{\infty} \frac{e^{-\frac{1}{2}(\frac{KTY}{\sigma})^2} \quad \frac{Y(KTX-\frac{1}{2})}{\sigma^2}}{\cosh Y/2} \, dy$$

This can be written as

$$n_{tL} = \frac{N_t KT}{\sigma\sqrt{8\pi}} \; e^{-\frac{(x+2KT)^2}{G}} \quad e^{-\{[4(\frac{KT}{\sigma})^2 x^2 + \sigma^2 - 4KTx]\frac{1}{G}\}}$$

$$\times \; e^{\frac{1}{2}} \int_{-\infty}^{\infty} \frac{e^{-\frac{1}{2}[(\frac{KTY}{\sigma})-m]^2} \; e^{m^2/2}}{\cosh Y/2} \, dy \qquad \text{B8}$$

Where $G = 2\sigma^2 + 8(KT)^2$ and $m = (\frac{x}{\sigma} - \frac{\sigma}{2KT})$ B8'

On the otherhand, the occupied trap density per unit energy range is

$$n_t(E) = \frac{N_t}{\sigma\sqrt{2\pi}} \; \frac{e^{-\frac{(E-E_t)^2}{2\sigma^2}}}{1+e^{\frac{(E-E_F)}{KT}}} \qquad \text{B9}$$

The energy E_{max} at which $n_t(E)$ is maximum can be found by putting $\frac{dn_t(E)}{dE} = 0$. This results

$$E_{max} - E_t = -\frac{\sigma^2}{KT} \left\{ \frac{1}{1+e^{\frac{E_F-E_{max}}{KT}}} \right\} \qquad \text{B10}$$

Expanding the right hand of B10 in Taylor series and taking only the first two terms we obtain

$$E_{max} - E_t = -\frac{\sigma^2}{KT}\left\{\frac{1}{2} - \frac{(E_F - E_{max})}{4KT}\right\}$$

Rearranging gives

$$E_{max} - E_t = \frac{\sigma^2(E_F - E_t - 2KT)}{\sigma^2 + 4(KT)^2} \qquad \text{B10'}$$

If we set $E_{max} = E_F$, this will result

$$E_{max} = E_F = E_t - \frac{\sigma^2}{2KT} \qquad \text{B11}$$

Expressing E_t as in Eq.B11, the concentration of trapped carriers (Eq.B8) will be

$$n_{tL} = \left\{e^{-\frac{(x+2KT)^2}{G}}\right\}\left\{\frac{N_t KT}{\sigma\sqrt{8\pi}}\, e^{\frac{1}{2}} \int_{-\infty}^{\infty} \frac{e^{-\frac{1}{2}\left(\frac{KTY}{\sigma}\right)^2}}{\cosh Y/2}\, dy\right\} \qquad \text{B12}$$

Following the definition made by Bonham[40]:

$$A = \frac{N_t KT}{\sigma\sqrt{8\pi}}\, e^{\frac{1}{2}} \int_{-\infty}^{\infty} \frac{e^{-\frac{1}{2}\left(\frac{KTY}{\sigma}\right)^2}}{\cosh Y/2}\, dy \qquad \text{B13}$$

we will get

$$n_{tL} = A\, e^{-\frac{1}{G}(x+2KT)^2} \qquad \text{B14}$$

The constant A is weakly depends on N_t and $\frac{\sigma}{KT}$ and can be written as

$A = CN_t$ where $0.27 \leq C \leq 0.6$ within the interval of $\frac{\sigma}{KT} = 2$ to 7[18,40].

Equating B14 with A2 gives

$$\frac{[x + 2KT]^2}{G} = \ln\left(\frac{e_o L^2 A}{\varepsilon k_1 k_2 V}\right) \qquad \text{B15}$$

i.e.,

$$x + 2KT = \sqrt{G \ln\left(\frac{e_o L^2 A}{\varepsilon k_1 k_2 V}\right)} \qquad \text{B16}$$

Substituting for x results

$$E_F = E_t + 2KT - \sqrt{G \ln\left(\frac{e_o L^2 A}{\varepsilon k_1 k_2 V}\right)}$$

Hence,

$$e^{\frac{E_F}{KT}} = \frac{n_{cL}}{N_c}\, e^{E_c/KT} = e^{\left(\frac{E_t}{KT}+2\right)}\; e^{-\frac{1}{KT}\sqrt{G \ln\left(\frac{e_o L^2 A}{\varepsilon k_1 k_2 V}\right)}} \qquad \text{B17}$$

Using B8' and rearranging Eq.B17 can be written as

$$n_{cL} = N_c\, e^{-\frac{E_t'}{KT}+2}\; e^{-\frac{1}{KT}\sqrt{2\sigma^2[1+(\frac{2KT}{\sigma})^2]\ln\left(\frac{e_o L^2 A}{\varepsilon k_1 k_2 V}\right)}} \qquad \text{B18}$$

In the situation when $E > E_t$ i.e., when injection level scans the upper portion of the distribution, (from 2.37)

$$n_{tL} = \frac{N_t}{\sqrt{\Pi}} \int_{-\infty}^{\infty} \frac{e^{-Y^2}}{1+e^{\frac{1}{KT}(-x+\sigma Y\sqrt{2})}}\, dy = \frac{N_t I}{\sqrt{\Pi}} \qquad \text{B19}$$

Where

$$Y = \frac{E - E_t}{\sigma\sqrt{2}} \quad \text{and} \quad X = E_F - E_t \qquad \text{B20}$$

Consider error function of ω.

$$\text{erf}\,\omega = \frac{2}{\sqrt{\Pi}} \int_0^{\omega} e^{-\xi^2} d\xi = \frac{2}{1+e^{\frac{-4\omega}{\sqrt{\Pi}}}} - 1 \qquad \text{B21}$$

From B21

$$\frac{1}{1+e^{\frac{-4\omega}{\sqrt{\Pi}}}} = \frac{1+\text{erf}\,\omega}{2} \qquad \text{B22}$$

Therefore, the denominator of the term in integral (B19) can be approximated by using B22. Hence,

$$I = \tfrac{1}{2} \int_{-\infty}^{\infty} e^{-y^2} [1+\text{erf}\,\omega] dy \qquad \text{B23}$$

Where $\omega = \frac{\sqrt{\Pi}}{4KT} (x-y\,\sigma\sqrt{2})$. This approximation will introduce an error not more than 4%[29]. Therefore,

$$I = \tfrac{1}{2} \int_{-\infty}^{\infty} e^{-y^2} dy + \tfrac{1}{2} \int_{-\infty}^{\infty} e^{-y^2} \text{erf}\,\omega \; dy \qquad \text{B24}$$

or

$$I = I_1 + I_2 \qquad \text{B25}$$

Where

$$I = \tfrac{1}{2} \int_{-\infty}^{\infty} e^{-} \; dy = \frac{\sqrt{\Pi}}{2} \qquad \text{B26}$$

and

$$I_2 = \tfrac{1}{2} \int_{-\infty}^{\infty} \text{erf}\,\omega \, dy = \frac{1}{\sqrt{\Pi}} \int_{-\infty}^{\infty} e^{-y^2} \int_0^{\omega} e^{-\xi^2} d\xi \, dy \qquad \text{B27}$$

$$\frac{dI_2}{dx} = \frac{1}{4KT}\, e^{-\frac{\pi x^2}{16(KT)^2}} \int_{-\infty}^{\infty} \{ e^{-\frac{2\pi\ \sigma^2}{16(KT)^2} y^2}\ e^{\frac{2\sqrt{2\pi}\ \sigma\ xy}{16(KT)^2}}\ e^{-y^2} \}\ dy \qquad B28$$

Let

$$m = \frac{\sigma\sqrt{2\Pi}}{4KT} \qquad B29$$

Then Eq.B28 when evaluated will give

$$\frac{dI_2}{dx} = \frac{1}{4KT}\sqrt{\frac{\Pi}{1+m^2}}\ e^{-\frac{m^2x^2}{2\sigma^2(1+m^2)}} \qquad B30$$

Integrating back results

$$I_2 = \frac{-\Pi\sigma}{4mKT\sqrt{2}} + \frac{\Pi\,\sigma\sqrt{2}}{4KTm}\ \{ \frac{1}{1+e^{\frac{-4sx}{\sqrt{\Pi}}}} \} \qquad B31$$

Where

$$s = \frac{m}{\sigma\sqrt{2(1+m^2)}} \qquad B32$$

Substituting for m and s from B29 and B32

$$I_2 = -\frac{\sqrt{\Pi}}{2} + \frac{\sqrt{\Pi}}{1+e^{-\frac{x}{KT\ell}}} \qquad B33$$

With

$$\ell = \sqrt{1+\frac{2\,\Pi\,\sigma^2}{16(KT)^2}} \qquad B34$$

Eq.B25 therefore gives

$$I = \frac{\sqrt{\Pi}}{1+e^{-\frac{x}{KT\ell}}} \qquad B35$$

From B37 and B19

$$n_{tL} = \frac{N_t}{1+e^{-\frac{x}{KT\ell}}} \qquad B36$$

i.e.,

$$n_{tL} = \frac{N_t}{1+e^{\frac{E_t-E_F}{KT\ell}}} \qquad B37$$

APPENDIX C

LAPLACE TRANSFORM OF $\psi(t)$

The Laplace transform of the function $\psi(t)$ is given by

$$\psi^*(s) = \int_0^\infty e^{-st}\,\psi(t)dt \qquad \text{C1}$$

For very small s, i.e., $s \to o$, the exponential term can be expanded into Taylor's series.

$$\psi^*(s) = \int_0^\infty \{1-st + \tfrac{1}{2}st^2 - \ldots\ldots\}\,\psi(t)dt \qquad \text{C2}$$

Neglecting higher orders of s

$$\psi^*(s) \simeq \int_0^\infty (1-st)\psi(t)dt = 1-s\bar{t} \qquad \text{C3}$$

where

$$\bar{t} = \int_0^\infty t\,\psi(t)dt \qquad \text{C4}$$

is the first integral moment of the distribution $\psi(t)$.

Hence,

$$\int_0^\infty e^{-st}\,\psi(t)dt \simeq \int_0^\infty (1-st)\psi(t)dt \qquad \text{C5}$$

$$\int_0^\infty (1-e^{-st})\psi(t)dt \simeq s\int_0^\infty t\psi(t)dt = s\bar{t} \qquad \text{C6}$$

Consider the integral $I = \int_0^\infty \psi(t)(1-e^{-st})dt$ C7

If the distribution function is given by

$$\psi(t) = \frac{C}{\Gamma(1+\alpha)}\,t^{-(1+\alpha)} \qquad \text{C8}$$

$$I = \frac{C}{\Gamma(1+\alpha)} \int_0^\infty \frac{(1-e^{-st})dt}{t^{1+\alpha}} \qquad C9$$

Feller has shown that for stable distributions[39]

$$s^\alpha = \frac{\alpha}{\Gamma(1-\alpha)} \int_0^\infty \frac{1-e^{-st}}{t^{1+\alpha}} dt \qquad C10$$

From this we can get $I = C\frac{s^\alpha}{\alpha}$

or $$I \sim Cs^\alpha \qquad C11$$

Therefore, combining Eqs. C3, C6 and C11 we will get

$$\psi(s) \simeq 1-Cs^\alpha \qquad C12$$

APPENDIX D

```
5      PRINT "Program :Space Charge Limited Current ."
10     REM *SCLCTR77*
20 !   PLOTTER IS 705,"HPGL"
30 !   OUTPUT 705;"VS7.5"
40    CSIZE 4,.6
50     VIEWPORT 20,108,20,80
60     WINDOW -5,7,-15,-4
70     PEN 1
80     CLIP -2,3.5,-14,-6
90    AXES 1.5,2,-2,-14
100   CLIP OFF
110   LORG 6
120   PEN 1
130   FOR N=.5 TO 2.0 STEP 1
140   MOVE N,-14.2
150   LABEL N
160   NEXT N
170   FOR C=1 TO 1.5
180   MOVE C,-14.2
190   LABEL C
200   NEXT C
210   MOVE 2.5,-14.2
220   LABEL 3
230   MOVE -.5,-5.7
240   LABEL "LOG J "
250   PEN 1
260   MOVE .2,-15.1
270   LABEL "Fig 5.4a:SCLC in a-TNF(at room temperature)"
280   MOVE -2.5,-16
290   LABEL "Sample AI"
300   LORG 8
310   FOR M=-12 TO -8 STEP 2
320   PEN 1
330   MOVE -2,M
340   LABEL M-1
350   NEXT M
360   MOVE 3.6,-13.5
370   LABEL "LOG V"
380   PEN 1
390   MOVE 4.0,-7.5
400   PEN 6
410   LABEL "I"
420   MOVE 4.2,-6.4
430   PEN 2
440   LABEL "II"
450    DIM X3(2,31)
460    FOR R=1 TO 2
470   FOR Z=1 TO 31
480   READ X3(R,Z)
490   NEXT Z
500   NEXT R
510   DATA 4,13,21,30,39,46,55,64,74,84,88,98,120,140,150,170,200,250,290,310,340
,370,450,530,580,710,760,850,920,990,1200
520   DATA 10,30,50,70,90,110,130,150,170,190,200,220,250,270,290,300,320,340
530   DATA 360,380,400,420,440,460,480,500,520,540,560,580,600
540   FOR Z=1 TO 31
```

```
560  A1=X3(1,Z)*3*1.E-12
570  B1=LOG(A1)
580  A2=X3(2,Z)
590  MOVE LOG(A2)-3.5,B1+13
600  LABEL "x"
610  NEXT Z
620  FOR V=1 TO 600
630  PEN 6
640  Q=1.6E-19
650  U=2
660  L=4*1.E-4
670  Nc=2.E+21
680  Nt=1.E+17
690  X1=.5
700  X2=3/4
710  Et=.29
720  S=.10
730  £=3.2*8.85*1.E-14
740  T=290
750  K=8.62*1.E-5
760  C=K*T
770  A=.4
780  D=(1+(6.28*S*S)/(16*K*K*T*T))^.5
790  H=(Q*L*L*Nt-£*V)^D
800  W=EXP(-(Et+(S*S/(2*C)))/C)
810  X=EXP(-Et/C)
820  PLOT LGT(V),LGT(£*U*Nc*W*V*V/(Nt*L*L))-2.9
830  NEXT V
840  PENUP
850  MOVE -10,-2
860  PEN 1
870  FOR V=10 TO 500
880  PEN 2
890  Q=1.6E-19
900  U=2
910  L=4*1.E-4
920  Nc=2.E+21
930  Nt=1.E+17
940  X1=.5
950  X2=3/4
960  Et=.29
970  S=.10
980  £=3.2*8.85*1.E-14
990  T=290
1000 K=8.62*1.E-5
1010 C=K*T
1020 A=.4
1030 D=(1+(6.28*S*S)/(16*K*K*T*T))^.5
1040 P=LOG((Q*L*L*A*Nt)/(£*X1*X2*V))
1050 Y=S*(P*2*1*1*(1+(4*K*K*T*T)/(S*S)))^.5
1060 W=EXP(-(Et+(S*S/(2*C)))/C)
1070 X=EXP(-Et/C)
1080 PLOT LGT(V),LGT((Q*U*Nc*V*X*(EXP(2))*(EXP(-Y/C)))/L)-6.50
1090 NEXT V
1100 PENUP
1110 FOR V=.015001 TO 200 STEP 25
1120 PEN 4
1130 J=V*2*1.E-11
1140 PLOT LGT(V),LGT(J)-0
1150 NEXT V
```

```
1     PRINT "SCLC DEPENDANCE ON TEMPERATURE"
10    REM *SCJTSe88*
20    CSIZE 4,.6
30    VIEWPORT 5,50,30,90
40    WINDOW 3.0,4.0,-12,-5
50    CLIP 3.125,4.0,-10,-5
60    AXES .125,1,3.125,-10
70    CLIP OFF
80    PEN 3
90    LORG 6
100   FOR N=3.250 TO 3.75 STEP .25
110   MOVE N,-10.1
120   LABEL N
130   NEXT N
140   MOVE 4.15,-9.45
150   LABEL "1000"
160   FOR I=4.05 TO 4.25 STEP .05
170   PLOT I,-9.99
180   NEXT I
190   PEN Up
200   MOVE -10,-20
210   PEN 3
220   MOVE 4.15,-10
230   LABEL "T(K)"
240   LORG 8
250   FOR M=-10 TO -6 STEP 2
260   MOVE 3.10,M
270   LABEL 10
280   MOVE 3.18,M+.4
290   LABEL M
300   NEXT M
310   MOVE 3.3,-4.7
320   LABEL "J(A)"
330   MOVE 5.5,-12.38
340   LABEL "Fig  :SCLC dependence on T for a-Se and a-TNF"
350   MOVE 4.16,-11.0
360   LABEL "a) For a-Se,sample BI"
370   DIM A(2,11)
380   FOR I=1 TO 2
390   FOR L=1 TO 11
400   READ A(I,L)
410   NEXT L
420   NEXT I
430   DATA 3.37,3.39,3.4,3.45,3.5,3.52,3.55,3.59,3.64,3.7,3.75
440   DATA 190,170,165,138,119,105,80,70,50,25,16
450   FOR L=1 TO 11
460   C=(8*1.E-10)*A(2,L)
470   D=(8*1.E-10)*A(2,10)
480   MOVE A(1,L),LGT(C)
490   LABEL "x"
500   NEXT L
510   MOVE A(1,10)+.3,LGT(D)-.1
520   LABEL "120v"
530   DIM B(2,13)
```

```
540  FOR I=1 TO 2
550  FOR L=1 TO 13
560  READ B(I,L)
570  NEXT L
580  NEXT I
590  DATA 3.73,3.70,3.68,3.66,3.64,3.61,3.6,3.56,3.55,3.47,3.41,3.37,3.35
600  DATA  89,118,145,197,250,280,300,350,440,600,740,892,1023
610  FOR L=1 TO 13
620  C=(1*1.E-8)*B(2,L)
630  D=(1*1.E-8)*B(2,13)
640  MOVE B(1,L),LGT(C)
650  LABEL "o"
660  NEXT L
670  MOVE B(1,1)+.25,LGT(D)-.3
680  LABEL "200v"
690  FOR T=260 TO 310
700  V=120
710  U=2
720  L=3*1.E-4
730  Nc=1.E+17
740  Nt=3*1.E+15
750  Et=.12
760  S=.06
770  £=5.4*8.85*1.E-14
780  K=8.62*1.E-5
790  C=K*T
800  H=EXP(-(Et+(S*S/(2*C)))/C)
810  R1=£*U*Nc*H*V*V/(Nt*L*L)
820  IF V>120 THEN 375
830  PLOT 1000/T,LOG(R1)-1.0
840  NEXT T
850  PENUP
860  MOVE -20,-20
870  PEN 1
880  FOR T=260 TO 310
890  V=120
900  U=2
910  L=3*1.E-4
920  Nc=1.E+17
930  Nt=3*1.E+15
940  Et=.12
950  S=.06
960  £=5.4*8.85*1.E-14
970  K=8.62*1.E-5
980  C=K*T
990  H=EXP(-(Et+(S*S/(2*C)))/C)
1000 R2=£*U*Nc*H*V*V/(Nt*L*L)
1010 PLOT 1000/T,LOG(R2)+.80
1020 NEXT T
1030 END
```

```
10    PRINT "Program used for simulating transient current"
20    REM *I(t)GAUS*
30   CSIZE 4,.6
40    VIEWPORT 10,100,10,120
50    WINDOW -20,10,90,130
60    PEN 1
70    CLIP -15,10,100,130
80   AXES 5,5,-15,100
90   CLIP OFF
100  LORG 6
110  MOVE -12.5,125
120  PEN 4
130  LABEL "LOG J"
140  MOVE 8,102
150  LABEL "LOG t"
160  MOVE -2,95
170 !PEN 6
180  LABEL "Fig.11: Trancient current for Gaus. distribution"
190  LORG 8
200 FOR Tt=1.E-6 TO 5.E-2 STEP 1.E-4
210 PEN 2
220   T=290
230   L=1.6E-3
240  A=1
250  K=100
260  S=.8
270  V=20
280  P=LOG(V/L)
290  H=LOG(T)
300  I=A+P+H+K+(S-1)*(LOG(Tt))
310  PLOT LOG(Tt),I
320  NEXT Tt
330  PEN Up
340  MOVE -50,-50
350  FOR Tt=5.0*1.E-2 TO 50 STEP 1.E-1
360  PEN 2
370  B=1.25*1.E+2
380  L=1.6E-3
390  V=20
400  T=290
410  S=.8
420  K=9.6
430  P=LOG(V/L)
440  H=LOG(T)
450  I=B-P+H-K-(S+1)*(LOG(Tt))
460  PLOT LOG(Tt),I
470  NEXT Tt
480  END
```

```
10   PRINT "PROGRAM FOR COMPUTING tr"
20    REM *DISPCHEC*
30   CSIZE 4,.6
40    VIEWPORT 10,100,10,100
50    WINDOW -13,-3,-8,5
60    PEN 2
70    CLIP -12,-3,-4,5
80   AXES 1,1,-12,-4
90   CLIP OFF
100  LORG 6
110  PEN 3
120  FOR N=-11 TO -4
130  MOVE N,-4.3
140  LABEL N
150  NEXT N
160  MOVE -3.4,-3.2
170  LABEL "LOGt"
180  PEN 2
190  MOVE -8.0,-5.4
200  LABEL "Fig14:Trancient current in Se"
210  MOVE -8.8,-6.2
220  LABEL "for diff. T & V=40"
230  LORG 8
240  FOR M=-4 TO 2
250  PEN 2
260  MOVE -12.0,M
270  LABEL M
280  NEXT M
290  MOVE -10.5,2.2
300  LABEL "LOG J"
310  PEN 4
320   DIM G(2,7)
330   FOR I=1 TO 2
340  FOR L=1 TO 7
350  READ G(I,L)
360  NEXT L
370  NEXT I
380  DATA 6.2,5.2,4.1,3.2,2.7,2.2,1.5
390  DATA .1,.2,.8,1.3,2,2.6,3.2
400  FOR L=1 TO 7
410  MOVE LOG(G(2,L)*.2*1.E-3),LOG(G(1,L)*.2)
420  LABEL "x"
430  NEXT L
440  FOR Tt=1.E-5 TO 1.E-3 STEP 1.E-5
450  PEN 3
460  A=10
470  V=10
480  D=4
490  T=291
500  K=100
510  F=(V/D)*1.E+4
520  P=LOG(F)
```

```
10    PRINT "Program used for computing activation energy Ea"
20    REM *U Vs T TRI*
30   CSIZE 4,.6
40    VIEWPORT 20,128,30,90
50    WINDOW 1,16,-9.0,-3.5
60    PEN 1
70    CLIP 2,7,-8,-3.5
80   AXES .5,1,2,-8
90   CLIP OFF
100  LORG 6
110  PEN 1
120  FOR N=2 TO 6 STEP 1
130  MOVE N,-8.1
140  LABEL N
150  NEXT N
160  MOVE 6.9,-3.2
170  LABEL "LOG U                    "
180  PEN 1
190  MOVE 7.9,-10.1
200  LABEL "Fig 5.9: Temperature dependece of drift"
210  MOVE 9.5,-10.5
220  LABEL "mobilities (at constant field)"
230  LORG 8
240  FOR M=-7 TO -4 STEP 1
250  MOVE 2.1,M
260  LABEL M
270  NEXT M
280  MOVE 16.0,-7.7
290  LABEL "1000/T(K)                    "
300  MOVE 14.7,-8.8
310  LABEL "a)Sample AII(TNF)                     "
320  MOVE 15,-9.4
330  LABEL "  (electrons)                       "
340   DIM G(2,8)
350   FOR I=1 TO 2
360  FOR L=1 TO 8
370  READ G(I,L)
380  NEXT L
390  NEXT I
400  DATA 2.1,2.6,5.6,10,12,25,37,67
410  DATA  0,3.5,12.5,21,25,32,37.5,50
420  FOR L=1 TO 8
430  A=G(1,L)*1.E-7
440  B=273.15+G(2,L)
450  MOVE 1000/B,LGT(A)
460  LABEL "x"
470  NEXT L
480 FOR X=2.6 TO 3.8 STEP .2
490 PLOT X,6.3-3.88*X
500 NEXT X
510 PENUP
520 MOVE 9,-2
530 PRINT "Ea=";3.88/(8.62*1)
540 END
```

```
10  PRINT "Program used for simulating field dependance of u"
20  REM *UVSFI*
30  CSIZE 4,.6
40   VIEWPORT 20,128,0,90
50   WINDOW -1,23,-9,-2.5
60   PEN 1
70   CLIP 0,7,-6,-3
80  AXES 2,1,0,-6
90  CLIP OFF
100 LORG 6
110 PEN 1
120 FOR N=0 TO 7 STEP 2
130 MOVE N,-6.1
140 LABEL N
150 NEXT N
160 MOVE 1.9,-2.8
170 LABEL "LOG U"
180 PEN 1
190 MOVE 10.5,-7.2
200 LABEL "Fig 5.10: Field dependence of drift mobilty"
210 MOVE 9.1,-7.6
220 LABEL "at room temperature"
230 LORG 8
240 MOVE 22.7,-6.6
250 LABEL "a) a-TNF.Sample AII                               "
260 FOR M=-5 TO -3 STEP 1
270 PEN 1
280 MOVE .3,M
290 LABEL M
300 NEXT M
310 MOVE 9,-5.8
320 LABEL "(F[v/m]) 10"
330 MOVE 9.6,-5.6
340 LABEL "1/2  3"
350 PEN 1
360  DIM G(2,5)
370  FOR I=1 TO 2
380 FOR L=1 TO 5
390 READ G(I,L)
400 NEXT L
410 NEXT I
420 DATA 1.5,2.5,5,8.3,12.5
430 DATA 2,2.75,4,4.8,5.5
440 FOR L=1 TO 5
450 A=G(1,L)*1.E-6
460 MOVE G(2,L),LGT(A)+1
470 LABEL "x"
480 NEXT L
490 FOR Q=.5 TO 5.5
500 PLOT Q,-5.3+.27*Q
510 NEXT Q
520 PENUP
530 END
```

```
10    PRINT "Program for estimating Ea from TSC measurement"
20    CSIZE 4,.6
30     VIEWPORT 0,80,30,90
40     WINDOW 2,4,-13,-9
50     PEN 1
60     CLIP 3.0,4,-12,-9
70    AXES .5,1,3.0,-12
80    CLIP OFF
90    LORG 6
100   PEN 1
110   FOR N=3 TO 4 STEP .5
120   MOVE N,-12.1
130   LABEL N
140   NEXT N
150   MOVE 4.2,-11.66
160   LABEL "1000/T,K"
170   MOVE 4.5,-11.5
180   LABEL "-1"
190   LORG 8
200   MOVE 3.25,-9
210   LABEL "J,A"
220   FOR M=-12 TO -10
230   B=10^M
240   MOVE 2.93,M
250   LABEL 10
260   MOVE 3.05,M+.2
270   LABEL M
280   MOVE 3,M+LGT(5)
290   LABEL 5
300   MOVE 3.03,M+LGT(5)
310   LABEL "-"
320   NEXT M
330   DIM A(2,5)
340   FOR I=1 TO 2
350   FOR L=1 TO 5
360   READ A(I,L)
370   NEXT L
380   NEXT I
390   DATA 290.0,301.0,308.5,313.0,316.0
400   DATA 1.4,3.5,8,10.5,12.3
410   FOR L=1 TO 5
420   D=LGT(A(2,L)*1.E-11)
430   C=1000/A(1,L)
440   MOVE C,D
450   LABEL "x"
460   NEXT L
470   PEN Up
480   MOVE -20,-1
490   FOR T=3.5 TO 3 STEP -.1
500   PLOT T,.3-3.28*T
```

```
510  NEXT T
520  K=8.62*1.E-2
530  R=EXP(1)
540  Y=LGT(R)
550  W=3.28*K/Y
560  MOVE 5,-9.5
570  LABEL W
580  MOVE 4.05,-9.5
590  LABEL "W="
600  END
```

BIBLIOGRAPHY

1. R. zallen The Physics of Amorphous Solids, 1983, John Wiley & Sons, U.S.A.

2. R.M. Schaffert Photography Science & Engineering 22, 3 (1978).

3. J.O.M. Bookris, D. Miller Conducting Polymers, 1987, Reidel Publishing Company, Netherlands, P. 1-31.

4. J. J. Miasik, A. Hopper, P.T. Moseley & B.C. To field Conducting polymers, 1987, Netherlands P. 189-193.

5. R. L. Emerald & J. Mort J. Appl. Phys.45,9(1974) 3943-3945

6. M.H. Brodsky Amorphous Semiconductors, 1985, Springer-Verlag, Germany p. 41-70.

7. E.A. Davis Amorphous Semiconductors, 1985, springer-verlag, Germany P.41-70.

8. V.I. Airhipov, V.A. Rolesnikov & A.I. Rudenko J. Phys D: Appl. Phys., 17(1984) 1241-1254.

9. S.R. Elliot Structure and Bonding In Non crystalline solids, 1986, Plenum press Newyork P.1-31.

10. G.R. Michell Order In the Amorphous State of Polymers, 1987, Plenum press, New York. P1-31.

11. G.Lucovisky & T.M. Hayes Amorphous Semiconductors, 1985, Springer-verlag, Germany P. 215-250.

12. A.J. Epstein, J.M. Ginder, A.F. Richer & A. Mucdiarmid Conducting Polymers, Netherlands, P.121-140.

13. P.D. Town send Conducting Polymers, Reidel Pub. Comp., Netherlands, p. 77-88.

14. K. Fesser J. Phy C: Solid state phy 21 (1988) 361-68.

15. Sworakowski, Nespurec J. Electrostatic 8(1979) 97-101.

16. Rizzo, Micoccia & Tepeie J. Appl. Phys., 48,8 (1977).

17. J.L. Hartke Physical review 125, 4 (1962) 1977

18. S. Nespureck & E.A. Silinish Phy Stat Sol(a) 34,747(1976).

19. S.Nespureck, P. Smejtek Czech. J. phys B 22(1972) 160-175.

20. H. Scher & W Montrol Physical review B12, 6(1975).

21. W.D. Gill J. Appl. Phys., 47 (1972) 5033-5039.

22. M.M. Sokolova & L.D. Rozenshtein Phys. Stat 50(a) 5,59(1975).

23. R.M. Blakney & H.P. Grunwald Physical review 159, 3(1967).

24. J.M. Marshal Phylosophical magazine, 36, 4, (1977).

25. P. Nagels Amorphous Semiconductors, 1985, Springer Verlag, Germany P. 113-158.

26. J. Fonash Solar cell device physics, 1981, Academic press, USA.

27. M. Shlesinger, J. Stat. Phys 10,42(1974).

28. R.B. Adler, A.C. Smith, R.L. Longini Introduction t o Semiconductor Physics, John Wiley Sons, New York.

29. B.D. Gupta Mathematical Physics, 1978, India.

30. J. Hirsch J. Phys. C:Solid state Phys, 12 (1979)321-325.

31. Bube Photoconductivity in Solids.

32. A. Bernes, R.F. Boyer, D. Chatain, C. Lacabunne & J . PIbar order In Amorphous "State" of Polymers, 1987 Plenum press, New York. P. 305-326.

35. I chen J. Appl. Phys. 47,2 (1976)

36. T. Mizatani, T. Yamada & M Ieda J. Phys. D:Appl. Phys. 14(1981)1139-47.

37. Abkowitz M.A. & Pfister. G. J. Appl. 46(1975)2559-73.

38. W. Feller An introduction to probability theory and its applications. Vol. II 2nd ed.John Wiley & Sons, New York.

40. J. Bonham Aust. J. Chem 26(1973)927-939.

41. Pfister & M. Scher Adv. Phys 27, 747 (1978)